Journal of proteome research

Article

pubs.acs.org/jpr

Quantitative Proteomics of Synaptic and Nonsynaptic Mitochondria: Insights for Synaptic Mitochondrial Vulnerability

Kelly L. Stauch, Phillip R. Purnell, and Howard S. Fox*

Department of Pharmacology and Experimental Neuroscience, University of Nebraska Medical Center, 985800 Nebraska Medical Center, Omaha, Nebraska 68198, United States

Supporting Information

ABSTRACT: Synaptic mitochondria are essential for maintaining calcium homeostasis and producing ATP, processes vital for neuronal integrity and synaptic transmission. Synaptic mitochondria exhibit increased oxidative damage during aging and are more vulnerable to calcium insult than nonsynaptic mitochondria. Why synaptic mitochondria are specifically more susceptible to cumulative damage remains to be determined. In this study, the generation of a super-SILAC mix that served as an appropriate internal standard for mouse brain mitochondria mass spectrometry based analysis allowed for the quantification of the proteomic differences between synaptic and nonsynaptic mitochondria isolated from 10-month-old mice. We identified a total of 2260 common proteins between synaptic and nonsynaptic mitochondria of which 1629 were annotated as mitochondrial. Quantitative proteomic analysis of the proteins common between synaptic and nonsynaptic mitochondria revealed significant differential expression of 522 proteins involved in several pathways including oxidative phosphorylation, mitochondrial fission/fusion, calcium transport, and mitochondrial DNA replication and maintenance. In comparison to nonsynaptic mitochondria, synaptic mitochondria exhibited increased age-associated mitochondrial DNA deletions and decreased bioenergetic function. These findings provide insights into synaptic mitochondrial susceptibility to damage.

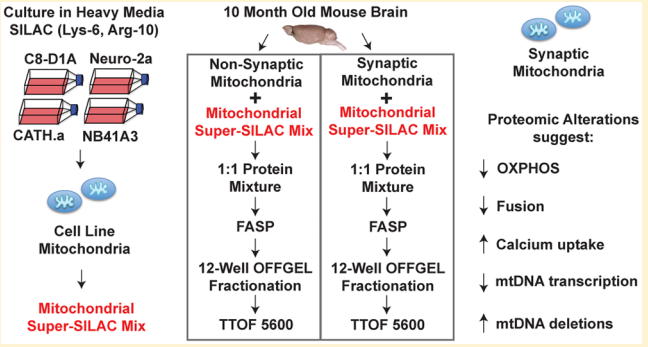

KEYWORDS: *neurons, synapse, mitochondria, oxidative phosphorylation, fission/fusion, calcium, mitochondrial DNA deletions*

INTRODUCTION

Mitochondria are energy-generating organelles that, in addition to producing ATP, play a vital role in the maintenance of intracellular calcium homeostasis and induction of apoptosis. Mitochondria are quite dynamic; they fuse, divide, and are transported within eukaryotic cells in response to various physiological cues. Increasing evidence suggests mitochondria in different cell types and different cellular compartments can exhibit heterogeneity in their function, trafficking patterns, lifespan, and morphology.[1,2] Mitochondrial heterogeneity as observed in neurons may facilitate unique requirements of the different cellular compartments. Neurons are polarized cells that consist of three distinct structural and functional domains: the cell body (soma), an axon, and complex dendrites with many branches and elaborate arbors. The formation of an axon−dendrite synaptic connection allows for interneuronal communication. Synaptic mitochondria are defined as those docked and aggregated in synapses which are sites of high-energy demand and extensive calcium fluctuations.[3,4] Thus, neuronal function and synaptic transmission rely largely on mitochondrial accumulation in synapses for energy production and maintenance of calcium levels.[5−7] Mitochondrial dysfunction and defects in mitochondrial fission and fusion are predicted to affect various aspects of neuronal physiology.[8,9] The occurrence of neurological defects associated with a great variety of diseases caused by mutations in genes encoding mitochondrial proteins further emphasizes the importance of neuronal mitochondria function.[9]

Mitochondrial biogenesis depends on nuclear encoded genes, and degradation machineries are primarily located in the perinuclear region of neuronal cytoplasm.[4,10] Therefore, synaptic mitochondria must be transported back and forth between the soma and synapses via mitochondrial transport systems. Mitochondrial fission/fusion cycles facilitate trafficking to and from the synapse, in addition to preserving the health of mitochondrial networks by facilitating degradation of the most damaged mitochondria.[6,11] The proper degradation of aged and damaged mitochondria through autophagy (termed mitophagy) is essential for neuronal survival and function. Synaptic mitochondria display a longer lifespan and increased vulnerability to cumulative damage than nonsynaptic mitochondria.[12] Synaptic mitochondria display increased oxidative damage during aging and are particularly susceptible to calcium insult.[12−14] Several hypotheses have been proposed to account for the increased vulnerability of synaptic mitochondria

Received: January 23, 2014
Published: April 7, 2014

   dx.doi.org/10.1021/pr500295n | J. Proteome Res. 2014, 13, 2620−2636

including relative isolation in comparison to clusters of mitochondria found in the neuronal soma, increased exposure to oxidative stress and calcium fluxes, older age, and high energy demands.[12,15−17] However, unraveling the link between the cause of synaptic mitochondrial vulnerability and the resulting cumulative damage has proven a complex task, particularly since mitochondria are dynamic organelles with interdependent functions. In the present work, we used quantitative mass spectrometry (MS) based analysis to examine the proteome differences between synaptic and nonsynaptic mitochondria in order to illuminate pathways that are necessary for important heterogeneous functions and contribute to the increased vulnerability of synaptic mitochondria.

Stable isotope labeling with amino acids in cell culture (SILAC), where cells are differentially labeled by growing them in "light" medium (normal amino acids) or "heavy" medium (containing stable isotope analogues that are substituted for certain amino acids) is an ideal method for accurate quantitative proteomics. The use of SILAC has recently been expanded to tissue analysis by using a mix of multiple SILAC-labeled cell lines as internal standards for tissue proteome quantification (termed super-SILAC).[18−20] Since our goal is to characterize alterations in the synaptic mitochondrial proteome, we first generated a super-SILAC mix and performed label-free proteomic analysis to validate its use as an appropriate internal standard for mouse brain mitochondria. The use of shotgun proteomics combined with the super-SILAC quantitative approach allowed for the identification of, in total, 2260 proteins common between synaptic and nonsynaptic mitochondria of which 1629 were annotated to be mitochondrial and 522 were found to be significantly differentially expressed. Potential proteomic differences responsible for the susceptibility of synaptic mitochondria to cumulative damage were identified. Orthogonal validation using Western blotting and the combination of Gene Ontology categories enrichment analysis and Ingenuity Pathway Analyses identified key processes and proteins important for neuronal function that are altered in synaptic mitochondria. Functionally, bioenergetic analysis revealed decreased respiration in synaptic mitochondria, which also exhibited an increased presence of mitochondrial DNA (mtDNA) deletions.

EXPERIMENTAL PROCEDURES

Animals

A total of 11 C57BL/6 male mice (substrain C57BL/6NCrl, 10 months old) were obtained from Charles River Laboratories International, Inc. Two were used for MS, six were used for Seahorse XF24 bioenergetic analysis, and the remaining three were used for electron microscopy and mtDNA mutation analyses. All protocols were implemented in accordance with NIH guidelines and approved by the Institutional Animal Care and Use Committee at the College of Medicine, University of Nebraska Medical Center. Animals were housed with a constant 12 h light/dark cycle in a controlled room and fed standard pellet mouse diet and water ad libitum.

Isolation of Synaptic and Nonsynaptic Brain Mitochondria

Synaptic and nonsynaptic mitochondria were isolated from 10-month-old C57BL/6 mice using a method modified from that described previously.[21] Following decapitation, brains were quickly removed and placed in ice-cold isolation medium (IM) containing 225 mM sucrose, 75 mM mannitol, 1 mM EGTA, 5 mM Hepes, and cOmplete Mini, EDTA-free protease inhibitor cocktail (Roche Diagnostics) adjusted to pH 7.4 with Tris-base. All homogenization and centrifugation steps were carried out on ice and at 4 °C, respectively. Brains were chopped into small pieces and homogenized with 35 strokes in a Dounce homogenizer. The homogenate was centrifuged at 1300*g* for 3 min, and then the supernatant was collected. The resulting pellet was resuspended in IM and centrifuged again at 1300*g* for 3 min. The pooled supernatants were centrifuged at 21000*g* for 10 min. This pellet was then resuspended in 15% Percoll and layered on top of a 24% and 40% Percoll gradient (prepared from 100% Percoll solution containing 225 mM sucrose, 75 mM mannitol, 1 mM EGTA, and 5 mM Hepes adjusted to pH 7.4 with HCl). After centrifugation for 8 min at 30700*g* the banding near the interface of the upper two layers of the gradient, which contains mainly synaptosomes, was collected and diluted in IM. The material accumulating at the interface between the 40% and the 24% Percoll solution, which is enriched with nonsynaptic mitochondria was also collected and diluted in IM.

The synaptosomal fraction was transferred to a nitrogen cavitation vessel (Parr Instrument Co.) where the pressure was equilibrated to 900 psi for 15 min followed by depressurization to ATM pressure releasing the synaptic mitochondria.[21] This suspension was then added to the top of 24% Percoll and centrifuged for 10 min at 30700*g*. The pellet containing the synaptic mitochondria was resuspended in IM. The resuspended synaptic and nonsynaptic mitochondria were centrifuged at 16700*g* for 10 min. Finally, the pellets were resuspended in IM with fatty acid free BSA followed by centrifugation at 6900*g* for 10 min. These final pellets, which contain synaptic or nonsynaptic mitochondria, were both further purified using an anti-TOM22 immunomagnetic affinity isolation (Miltenyi Biotech). Resulting mitochondria were lysed in 100 mM Tris-HCl with 4% (w/v) SDS and 0.1 M DTT adjusted to pH 7.6. Lysates were incubated at 95 °C for 5 min and then briefly sonicated. Protein concentrations were determined using a Pierce 660 nm Protein Assay (Thermo Scientific).

Identification of Mitochondria with Electron Microscopy

Isolated synaptic and nonsynaptic mitochondria were fixed overnight in 2.5% glutaraldehyde in 0.1 M cacodylate buffer, pH 7.4 at 4 °C, postfixed with 1% cacodylate-buffered osmium tetraoxide for 2 h at room temperature, and then dehydrated in a graded series of ethanol, briefly transferred to propylene oxide, and embedded in Epon-Araldite. Routine thin-section ultrastructural analysis was performed as described previously.[22] Sections were stained with uranyl acetate and lead citrate, and then randomly selected noncontiguous, nonoverlapping, digitized images of each mitochondrial pellet (21000 and 52000× magnification) were captured on a FEI Tecnai G2 Spirit transmission electron microscope. Mitochondria were classified as intact by visualization of condensed cristae and an uninterrupted outer membrane.

Cell Culture and Mitochondrial Super-SILAC Mix Preparation

The mouse cell lines Neuro-2a, CATH.a, NB41A3, and C8-D1A were obtained from ATCC. The cells were grown in DMEM/F-12 media supplemented with fetal bovine serum, L-glutamine, and penicillin−streptomycin. At 80% confluency, cells were rinsed twice with PBS, collected, pelleted, and flash frozen in liquid nitrogen followed by storage at −80 °C. Mitochondria were isolated from lysed cells by sequential

dx.doi.org/10.1021/pr500295n | J. Proteome Res. 2014, 13, 2620−2636

differential centrifugation using the Mitochondrial Isolation Kit for Cultured Cells (Mitosciences) followed by anti-TOM22 immunomagnetic isolation (Miltenyi Biotech). For stable-isotope labeling by amino acids in cell culture (SILAC) experiments, the four cell lines were SILAC-labeled by culturing in Advanced DMEM/F-12 (Invitrogen) in which the natural lysine and arginine were replaced by heavy isotope-labeled amino acids, (U-$^{13}C_6{}^{15}N_4$)-L-arginine (Arg-10) and (U-$^{13}C_6$)-L-lysine (Lys-6) supplemented with 10% dialyzed fetal bovine serum, SILAC glucose solution, L-glutamine, SILAC phenol red solution, and penicillin−streptomycin. Cells were cultured for at least seven generations in the SILAC media until fully labeled as assessed by quantitative MS. The mitochondrial super-SILAC mix was prepared by mixing equal amounts of each of the four cell lines of heavy mitochondrial lysate which were then combined with unlabeled lysate from either the synaptic or nonsynaptic mitochondria isolated from mouse brain as described above.

Protein Digestion and Fractionation

The filter-aided proteome preparation technique[23] with a 20-μm filter (Pall Corporation) was used for protein trypsinization. The resultant peptides were cleaned with an Oasis mixed-mode weak cation-exchange cartridge (Waters). Peptides were quantified using a NanoDrop 2000 UV−vis Spectrophotometer (Thermo Scientific) in conjunction with the Scopes method for protein quantification.[24] Isoelectric focusing was performed using an Agilent 3100 OFFGEL Fractionator with the pH 3−10 low-resolution kit (Agilent Technologies). Fractions were prepared for MS with Pierce C-18 PepClean Spin Columns (Thermo Fisher) in accord with manufacturer's instructions. Samples were dried with a Savant ISS 110 SpeedVac Concentrator (Thermo Fisher) and resuspended in 6 μL of 0.1% formic acid for LC−MS/MS analysis. Two independent biological replicates were performed for each synaptic and nonsynaptic preparation.

LC−MS/MS and Data Analysis

MS was conducted using an Eksigent ultra nano-HPLC with a cHiPLC system connected to an AB Sciex TripleTOF (TTOF) mass spectrometer equipped with a nanospray configuration (AB Sciex). Samples were loaded onto a 200 μm × 6 mm ChromXP C18-CL 3 μm 120 Å trap column (Eksigent), washed with 98:2 LC-MS water with 1% formic acid for 10 min, and then eluted through a 200 μm × 15 cm ChromXP C18-CL 3 μm 120 Å analytical column (Eksigent) at 300 nL/min with a linear gradient of acetonitrile from 0 to 60% over the course of 90 min. β-Galactosidase standards (25 fmol) were used for calibration. Peptide and protein lists were generated by analyzing TTOF data obtained with Protein Pilot version 4.5 (Paragon Algorithm: 4.5.0.0, 1654) software. Using the paragon method,[25] the peak lists were compared against the Uniprot 2013_07 release of 26-June-2013 of UniProtKB/Swiss-Prot containing 540546 sequence entries with contaminants added. The search parameters were set as a maximum of two missed cleavages, carbamidomethyl (C) as fixed modification, *N*-acetyl (protein) and oxidation (M) as variable modifications, top 6 MS/MS peaks per 100 Da, and MS/MS mass tolerance of 0.5 Da. The Protein Pilot search effort was set to "Thorough ID" and the False Discovery Rate Analysis was engaged, with the default setting for 'Detected Protein Threshold (Unused ProtScore (Conf))' at >0.05 (10.0%). Exclusion criteria to remove proteins from analysis were as follows: FDR of 0.05 for both peptides and proteins, peptides must contain at least 6 amino acids, contaminants as identified through the database search and proteins identified as being in the reverse database. The additional cutoff values of Unused ProtScore ≥1.3 and number of unique peptides ≥2 were applied to the data. Quantification was performed using the heavy super-SILAC mix as an internal standard and ratios were normalized to this mix and expressed here as light-to-heavy (L/H, sample/super-SILAC internal standards). To select proteins that show differential expression, our data was uploaded to the Cyber-T Web server (http://cybert.ics.uci.edu/),[26] which implements a *t* test using a Bayesian regularization method for quantitative MS analysis and multiple tests corrections were employed to derive the Posterior Probabilities of Differential Expression (PPDE) and perform Benjamini and Hochberg (BH) corrections. Cutoffs for proteins deemed as significantly differentially expressed were p values ≤0.05, PPDE values ≥0.95, and BH corrected q values (FDR) ≤ 0.05.

The synaptic and nonsynaptic mitochondria were compared as follows. First, protein ratios were determined against the super-SILAC internal standard for each of the mitochondrial samples (synaptic and nonsynaptic), which are expressed as L/H. Then, we determined the "ratio of ratio" value, which is the change in protein expression between the synaptic and nonsynaptic mitochondria. The heat maps represent the changes in protein expression levels in synaptic mitochondria relative to nonsynaptic mitochondria. The protein expression changes were imported into a multiple experiment viewer (Dana-Faber Cancer Institute). The heat maps were generated by this program and the color scale was set to encompass all values. All statistical analysis and linear fits were completed using Excel (Microsoft) and Prism (GraphPad Software).

Bioinformatic Analysis

Hierarchical clustering and principal component analyses of proteins were performed using Partek Genomics Suite 6.6 version 6.12.0713 software. MitoMiner v3.1−2013_10 (MRC: Mitochondrial Biology Unit; mitominer.mrc-mbu.cam.ac.uk) was used to annotate our identified and quantified proteins as mitochondrial. Categorical annotation was supplied in the form of Gene Ontology (GO) biological process, molecular function, and cellular component as defined by the Database for the Annotation, Visualization, and Integrated Discovery (DAVID; http://david.abcc.ncifcrf.gov/).[27] The DAVID EASE score is calculated using one-tail Fisher Exact probability values for gene-enrichment analysis. The Ingenuity Pathway Analysis (IPA; Ingenuity Systems; http://www.ingenuity.com) Upstream Regulator and Downstream Effects Analysis tool was used to predict alterations in the activity of mitochondrial transcriptional regulators based on our uploaded protein expression data.

Immunoblotting

Equal amounts of mitochondrial lysates prepared as described above (15 μg) were loaded onto 4−12% Bis-Tris gels, transferred to nitrocellulose membranes, blocked, and incubated with the following antibodies overnight at 4 °C: the oxidative phosphorylation (OXPHOS) panel (1:5000) (MS604; Mitoscences), VDAC1 (1:10,000) (4661; Cell Signaling), GAPDH (1:10,000) (437000; Invitrogen), ATP5H (1:10,000) (MS504; Mitosciences), MCU (1:1,000) (HPA016480; Sigma-Aldrich), MFN1 (1:2,000) (ab57602; Abcam), TFAM (1:4,000) (LS-C30495; LifeSpan Biosciences), and Synaptophysin (1:1,000) (4329; Cell Signaling). The OXPHOS antibody panel is a mix of antibodies that include

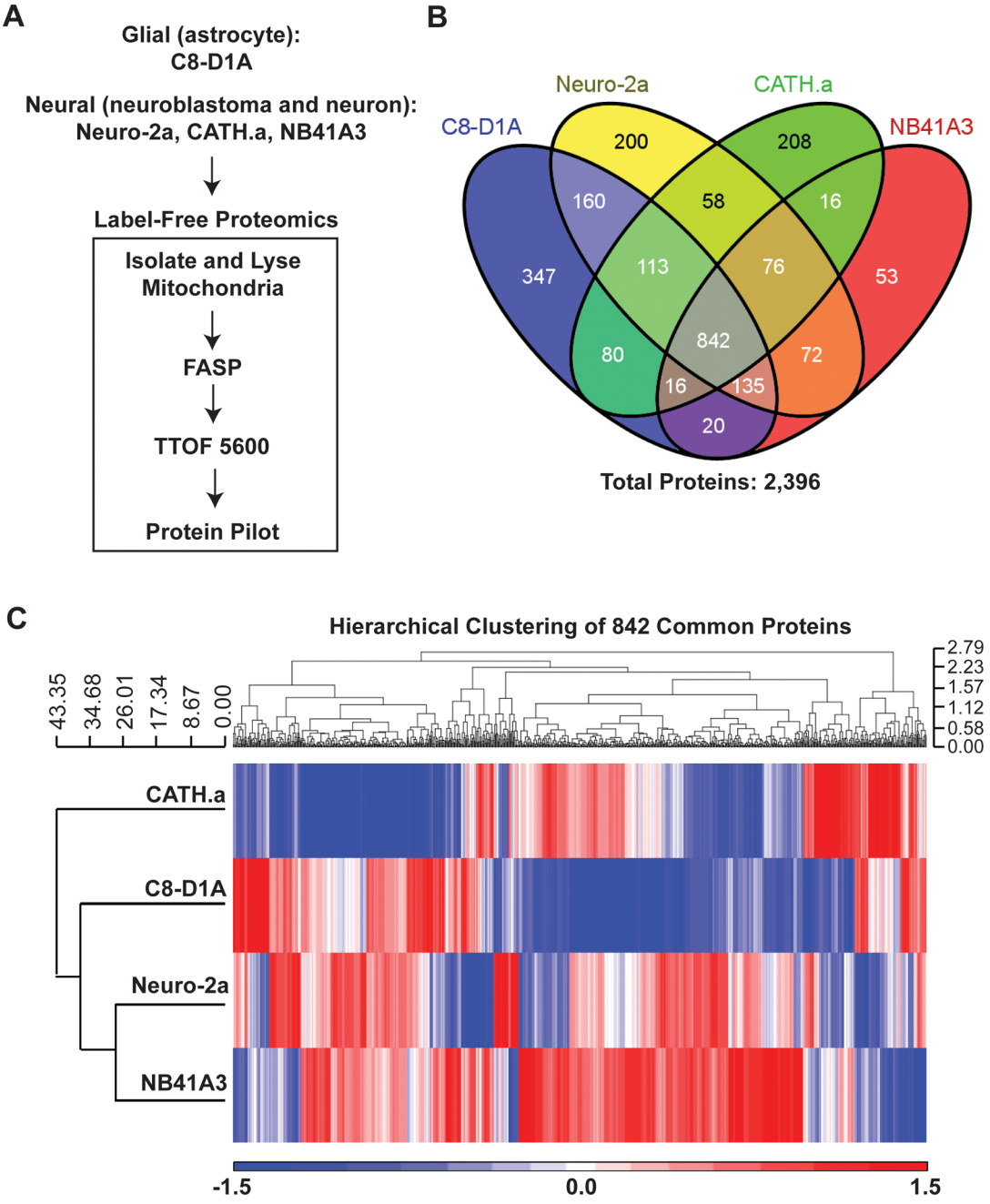

Figure 1. Generation of a mouse brain mitochondrial super-SILAC mix. (A) Label-free proteomics of isolated mitochondria from four mouse cell lines was performed after FASP processing and LC-MS/MS on a TTOF 5600. (B) Venn diagram of the common and unique proteins that were identified and quantified from the isolated mitochondria from each of the four cell lines. (C) Hiearchical clustering of the 842 common proteins using normalized spectral counts. The values are displayed on a $\log_{10}$ scale.

NDUFB8, SDHB, UQCRC2, COXI, and ATP5A1. The expression of mitochondrial proteins (VDAC1 and GAPDH) commonly used as loading controls have been shown to exhibit expression changes in response to different conditions[28,29] and in our proteomics; therefore, we performed Coomassie staining to confirm equal protein loading (Figure S1, Supporting Information). As revealed by our proteomics, VDAC1 expression is significantly decreased in synaptic mitochondria ($\log_2 = -0.42$, $p = 0.015$, PPDE = 0.96, BH = 0.039); however, VDAC1 immunoblotting was included to show consistent loading between all Western blots despite expression changes. Confirmation of equal protein loading for each membrane was performed by Ponceau staining. Chemiluminescent bands were visualized with an Image Station 4000MM Pro and analyzed using Carestream Molecular Imaging software (both from Carestream Health, Inc.).

Isolation and Bioenergetic Analysis of Isolated Brain Mitochondria

Synaptic and nonsynaptic mitochondria were isolated from 10-month-old mice as described above with the following modifications. The mouse brains were homogenized in mitochondrial isolation buffer (MSHE+BSA): 70 mM sucrose, 210 mM mannitol, 5 mM HEPES, 1 mM EGTA and 0.5% (w/v) fatty acid free BSA (pH 7.2) using only 10 strokes in a Dounce homogenizer. Following the Percoll centrifugation, the

dx.doi.org/10.1021/pr500295n | J. Proteome Res. 2014, 13, 2620−2636

final centrifugation steps were performed at 8000*g* for 10 min. The anti-TOM22 immunomagnetic affinity isolation purification step was not performed. Final pellets for bioenergetic analysis were resuspended in a minimal volume of MSHE + BSA. Total mitochondrial concentrations were determined using the BCA method. Isolated mitochondria were used immediately for analysis.

The Seahorse XF24 Flux Analyzer (Seahorse) was equilibrated to 37 °C overnight, and a modified protocol was used based on previous work in mouse liver mitochondria.[30] The isolated synaptic and nonsynaptic mitochondria (10 μg) were plated in V7-PS XF24 cell culture microplates in a volume of 50 μL mitochondrial assay solution (MAS) containing 10 mM pyruvate, 2 mM malate, and 4 μM FCCP as substrate for the electron flow experiment. After centrifugation for 15 min at 2000*g* to attach mitochondria, 450 μL of MAS (containing substrate) was added to each well, and the plate was incubated at 37 °C for 8 min to equilibrate temperature. The final concentrations of additions to the wells were 2 μM rotenone, 10 mM succinate, 4 μM antimycin A, and 10 mM ascorbate with 100 μM TMPD for the electron flow assay. The electron flow assay was run in 3−4 technical replicate wells for each independent biological replicate (n = 6). XF24 data was calculated using the algorithm previously described and used by the Seahorse software package.[31] Statistical analysis conducted in PRISM (GraphPad Software) using one-way ANOVA and post-test with Tukey's multiple comparison test.

PCR mtDNA Deletion Assay

To anneal DNA segments flanking three-direct repeats in the regions 8884−13357 oligonucleotide primers were synthesized (Eurofins MWG Operon).[32] For this, mtDNA was prepared from the synaptic and nonsynaptic mitochondrial fractions using the QIAamp DNA Micro Kit (Qiagen); the oligonucleotide outer primers, 5′-TAATTCAAGCCTACGTATTC-3′ (forward) and 5′-GGGATGTTTTTAGGCTTAGG-3′ (reverse), and oligonucleotide nested primers, 5′-CAAGTCCATGACCATTAACTGG-3′ (forward) and 5′-GATTTTATGGGTGTAATGCG-3′ (reverse), were used for the mtDNA deletion PCR reaction. The mtDNA segment (471−670) encoding 12S rRNA was also amplified as undeleted mtDNA controls in each sample, using 5′-GACAGCTAAGACCCAAACTG-3′ (forward) and 5′-TTAGCAAGAGATGGTGAGGT-3′ (reverse) primers. PCR conditions were initial denaturation at 94 °C for 4 min, followed by 30 cycles of denaturation, annealing, and extension at 94 °C for 20 s, 55 °C for 20 s, and 72 °C for 20 s, respectively, and final extension at 72 °C for 4 min; the FastStart High Fidelity PCR System, dNTPack (Roche) was used. The outer primers were used for the first 30 cycles as described above with 20 μg mtDNA template, followed by transfer of 2 μL of the first reaction to the nested PCR for the second 30 cycles. Resulting products were visualized by agarose gel electrophoresis.

RESULTS

Label-Free Proteomic Analysis for Development of a Mouse Brain Mitochondrial Super-SILAC mix

To accurately quantify proteome differences between synaptic and nonsynaptic mitochondria, we set out to generate a super-SILAC mix that would be appropriate as a comprehensive proteomic standard for mouse brain mitochondria. This is of particular importance because variations in the mitochondrial proteome have been observed among different cells, tissues, and disease states.[33−35] We chose the following mouse cell lines: the neuroblastoma derived cell lines, Neuro-2a and NB41A3, the immortalized neuronal cell line, CATH.a, and C8-D1A, a cell line with astrocytic properties. We first performed label-free proteomic analysis of mitochondria isolated from each cell line using sequential differential centrifugation and immunomagnetic affinity purification (Figure 1A). Mitochondrial protein lysate was trypsinized using the filter-aided sample preparation (FASP) method[23] and subjected to MS using a TTOF 5600 system (AB Sciex). Protein identification and spectral counts were determined using ProteoIQ software. The protein spectral counts, which are the total number of MS/MS spectra taken on peptides from a given protein in a given LC−MS/MS analysis, were further normalized by total spectral count. Using the Paragon algorithm,[25] 2396 proteins were identified from the mitochondria from the four cell lines in total, which resulted in the identification of more than 1200 proteins in each cell line (Figure 1B). The complete LC−MS/MS spectral count data for all proteins identified using mitochondria isolated from each of the four cell lines are provided in the Table S1A, Supporting Information. A total of 842 proteins were identified in all cell lines (35.1% of all identified proteins), and 39.6% protein identifications were shared between at least two proteomes (Figure 1B). The complete list of the 842 common identified proteins is provided in Table S1A, Supporting Information. To compare the proteomes of the cell lines to each other, we performed hierarchical clustering of the 842 common proteins using normalized spectral counts to reveal the degree of differences in protein expression patterns at a global level. This revealed that CATH.a and C8-D1A show the greatest dissimilarity (Figure 1C). Neuro-2a and NB41A3, the two neuroblastoma derived cell lines, were found to be the most similar (Figure 1C). To confirm and expand the hierarchical clustering results, we performed principal component analysis (PCA) of the spectral counts for all identified proteins in all samples. PCA transforms large data sets into points in a data space of orthogonal components, such that the first component has the largest possible variance. This analysis confirmed that CATH.a and C8-D1A were the furthest apart in this data space and supports that our mixture of cell lines consists of diverse proteomes (Figure S2A, Supporting Information). As a final examination of the level of similarity of the protein expression patterns between the different cell lines we calculated their Pearson correlation coefficients (r), which further confirmed the highest similarity between Neuro-2a and NB41A3 (Figure S2B, Supporting Information). Although the above analyses revealed that using a mixture of the four cell lines indeed captures diversity important for proteomic analysis, they do not provide evidence for mitochondrial proteome enrichment.

Therefore, we classified the 2396 identified proteins with MitoMiner, a database of the mitochondrial proteome, which annotated 1497 proteins (62.5% of all identified proteins) as mitochondrial (Figure 2). The MitoMiner annotated proteins identified using mitochondria from each of the four cell lines is provided in Table S1B (Supporting Information). As shown in Figure 2, unique mitochondrial proteins were identified in each of the four cell lines (154 from C8-D1A, 79 from Neuro-2a, 75 from CATH.a, and 29 from NB41A3, which corresponds to 10.3%, 5.3%, 5.0%, and 1.9% of all identified proteins, respectively), further validating the use of this mix of four mitochondrial proteomes. The MitoMiner annotated proteins identified as in common as well as unique to mitochondria

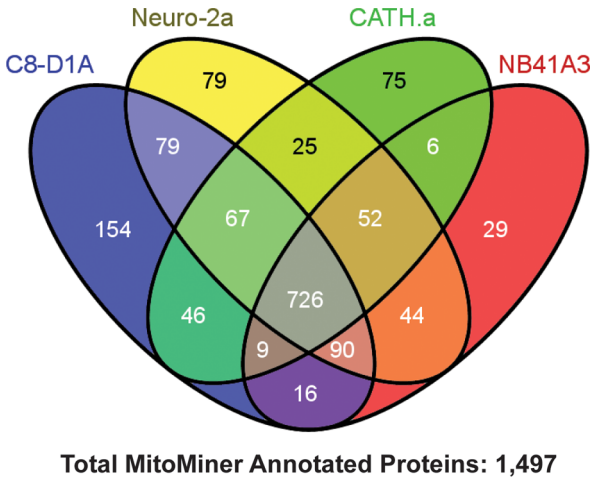

Figure 2. MitoMiner annotated proteins. Venn diagram of the common and unique proteins that were annotated to be mitochondrial by MitoMiner from mitochondria isolated from each of the four cell lines.

isolated from each of the four cell lines are provided in Table S1B (Supporting Information). Although the enrichment of mitochondrial-localized proteins is not 100%, it should be noted that proteins currently annotated as nonmitochondrial may indeed be false negatives, as the ability to localize proteins to mitochondria continues to increase.[36] The discrepancy can be explained due to the fact that the functional annotation of proteins is incomplete and constantly being updated. These results indicated that the use of a mixture of isolated mitochondria from these four cell lines provides enough similarity and diversity to adequately represent the mitochondrial proteome.

Quantitative Analysis of Synaptic and Nonsynaptic Mitochondrial Proteomes Using the Mitochondrial Super-SILAC Mix

To examine the differences in the synaptic and nonsynaptic mitochondrial proteomes, two male 10-month-old (considered to be the beginning of adult middle age in mice, approximating a 38-year old human[37]) littermate C57BL/6 mice were applied to our studies. First, synaptic and nonsynaptic mitochondria were prepared from mouse brain tissue using Percoll density gradient centrifugation to obtain "free" nonsynaptic mitochondria and synaptosomes, and synaptic mitochondria were released from synaptosomes by nitrogen cavitation as previously described.[21] The purity of synaptic and nonsynaptic mitochondria was determined using Western blot analysis for the enrichment of mitochondrial markers and relative absence of the soluble cytosolic protein GAPDH, as well as blotting for synaptophysin to verify enrichment of synaptosomes (Figure S3A, Supporting Information). Transmission electron microscopy using previously described ultrastructural criteria confirmed the isolated synaptic and nonsynaptic mitochondria were pure and intact (Figure S3B, Supporting Information).[38]

Second, to create the mitochondrial super-SILAC mix from the four selected cell lines we grew them in heavy (containing $^{13}C_6$ $^{15}N_4$-L-arginine and $^{13}C_6$-L-lysine) SILAC media and mixed the isolated mitochondrial lysates in equal proportions. The heavy isotope-labeled cell line mitochondrial proteins were used as internal standards to allow for comparison between unlabeled experimental groups (synaptic and nonsynaptic mitochondria). Isolated synaptic and nonsynaptic mitochondria were lysed and the proteins were mixed in a 1:1 ratio with the mitochondrial super-SILAC mix prior to FASP, 12-Well OFFGEL fractionation, and acquisition of data on a TTOF 5600. Joint analysis of the resulting 24 LC-MS/MS files (12 fractions for both synaptic and nonsynaptic mitochondrial samples for each of the two mice) in ProteinPilot using the Paragon algorithm identified a total of 2260 common proteins in both the synaptic and nonsynaptic mitochondria (Figure 3A). The complete super-SILAC data for all proteins identified using synaptic and nonsynaptic mitochondria isolated from mouse 1 and 2 as well as from the joint analysis are provided in Table S1C (Supporting Information). Hierarchical clustering of the 2260 common proteins using the normalized protein expression values (L/H) obtained using the heavy super-SILAC mix as an internal standard for each of the mitochondrial samples (synaptic and nonsynaptic) shows the global proteome differences between synaptic and nonsynaptic mitochondria (Figure 3B). To evaluate the enrichment of mitochondria-localized proteins within the synaptic and nonsynaptic mitochondrial proteomes, we uploaded our list of 2260 common proteins to the MitoMiner database. The MitoMiner database annotated 1869 proteins as mitochondrial, and of these, 1629 proteins are common to both synaptic and nonsynaptic mitochondria (Figure 3C). The complete super-SILAC data for all proteins identified as in common between synaptic and nonsynaptic mitochondria isolated from mouse 1 and 2 as well as the joint analysis including those annotated as mitochondrial using MitoMiner are provided in Table S1D (Supporting Information). Throughout the remainder of this paper, the term "mitochondrial proteins" will refer only to the MitoMiner annotated mitochondrial proteins. Although MS-based technical limitations may result in missing low-abundance mitochondrial proteins and mitochondrial proteins expressed only in specific tissues, developmental states, or cellular conditions and may not be captured due to limitations of our super-SILAC mix proteome coverage, we achieved 58.5% coverage of the mouse mitochondrial proteome (2783 mitochondrial proteins currently annotated by the MitoCarta Inventory of Mammalian Mitochondrial Genes). At this depth of proteome coverage, we exceed current MS-based mitochondrial protein identification as similar studies have only captured between 23 and 40% of known mitochondrial components.[39]

Although joint analysis identified 2260 proteins in common between synaptic and nonsynaptic mitochondria, independent analysis of the resulting 12 LC-MS/MS files for each of the two mice identified only 1720 and 1684 proteins in common between synaptic and nonsynaptic mitochondria (Figure 4A and B). Of these proteins, 1619 were identified and quantified in both biological replicates (Figure 4C), and 1278 were annotated as mitochondrial using MitoMiner (Figure 4D). Reproducibility is an important concern for quantitative proteomic studies. Therefore, to confirm the reproducibility of the proteomic experiment, two independent biological replicate preparations of proteins were performed for both synaptic and nonsynaptic mitochondria. There was a high correlation (the Pearson correlation coefficient r = 0.96 (synaptic) and 0.94 (nonsynaptic)) between the two biological replicate samples for both mitochondrial populations (Figure 5A,B). Additionally, the "ratio of ratio" distribution, which is the change in protein expression between the two biological replicates, resulted in curves generally composed of a normal distribution centered at $\log_2$ 0, consistent with normalized protein abundance ratios, thus further correction was not

dx.doi.org/10.1021/pr500295n | J. Proteome Res. 2014, 13, 2620−2636

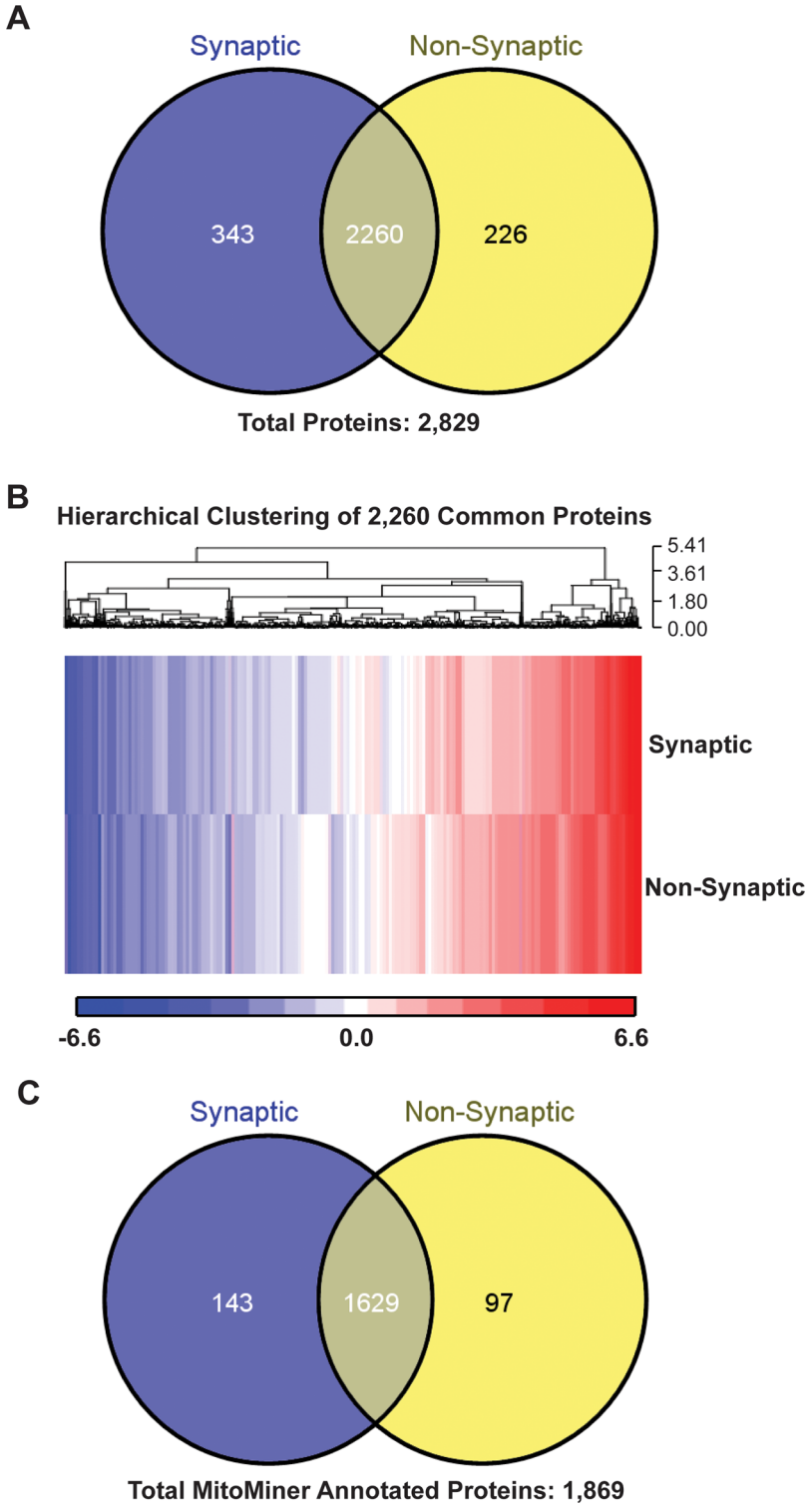

Figure 3. Global proteomics results obtained from super-SILAC experiment. (A) Venn diagram of the common and unique proteins that were identified and quantified from synaptic and nonsynaptic mitochondria. (B) Hierarchical clustering of the expression levels of the 2260 common proteins. The values are displayed on a $\log_2$ scale. (C) Venn diagram of the common and unique proteins that were annotated to be mitochondrial by MitoMiner from the synaptic and nonsynaptic mitochondria.

performed (Figure 5C,D). The high correlation of protein expression values between independent biological replicate samples indicated that the use of the super-SILAC technique for quantitative proteomic yields high reproducibility and accuracy, as reported previously.[18,19] These results also revealed that global proteomic differences exist between synaptic and nonsynaptic mitochondria isolated from 10-month-old mouse brain.

As with all quantitative MS-based experiments, the prevalence of missing data presents a challenge. Although missing values can be replaced by an imputed value, determining reasonable imputed values can be difficult in MS

dx.doi.org/10.1021/pr500295n | J. Proteome Res. 2014, 13, 2620−2636

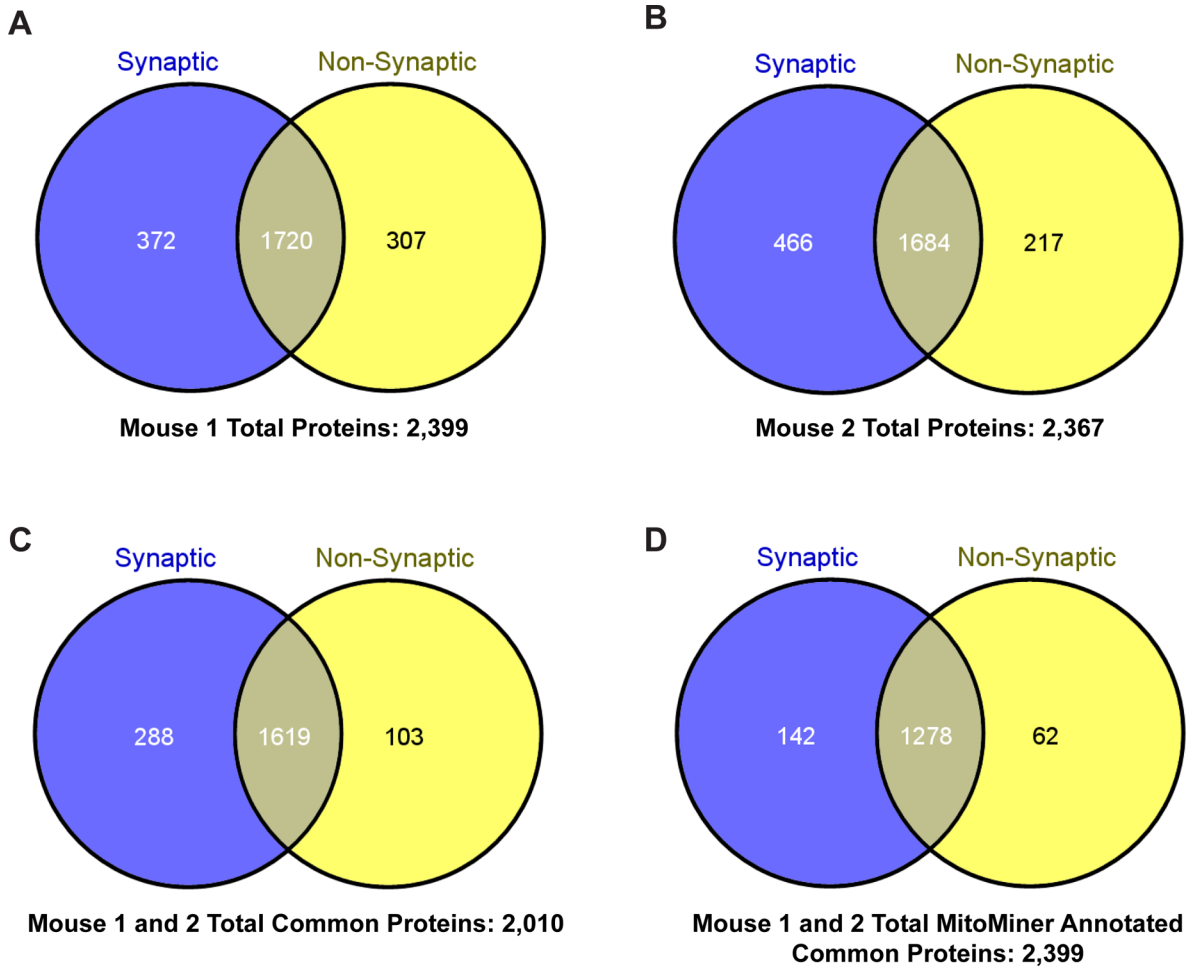

Figure 4. Comparison of identified synaptic and nonsynaptic mitochondrial proteins. Venn diagram of the common and unique proteins that were identified and quantified from synaptic and nonsynaptic mitochondria isolated from (A) mouse 1 and (B) mouse 2. (C) Common and unique proteins that were identified and quantified from synaptic and nonsynaptic mitochondria from both mouse 1 and 2. (D) Common and unique proteins that were annotated as mitochondrial by MitoMiner from synaptic and nonsynaptic mitochondria from both mouse 1 and 2.

based shotgun proteomics experiments.[40,41] If the peptide intensity value is truly present at an abundance the instrument should be able to detect it, but if it is not detected or is incorrectly identified, then using observed values to impute missing data or ignoring a few missing values is appropriate. However, if a peptide intensity value is missing due to abundance below the instrument's detection limits or the peptide is not present, then simple imputations based on observed values are not appropriate as this will lead to biased results.[42] The absence of peptide intensity values from one replicate sample does not necessarily indicate that the peptide is not present or below the detection limit; the value may be below the confidence limit set for the analysis. Therefore, the joint analysis of the LC−MS/MS files increases the number of spectra contributing to the quantitation of the peptide thus raising the confidence in the protein to meet the threshold set in ProteinPilot. We chose to address this situation by joint analysis of the 24 LC−MS/MS files from each biological replicate for each mitochondrial pool (synaptic or nonsynaptic) which resulted in only 21, 29, 22, and 24 missing values for mouse 1 nonsynaptic, mouse 2 nonsynaptic, mouse 1 synaptic, and mouse 2 synaptic mitochondria, respectively. Lists of the proteins identified as unique due to missing values in another sample are provided in Table S1E (Supporting Information).

As mentioned above, if the value was missing from both replicates or from only one mitochondrial pool (synaptic or nonsynaptic), the absence was assumed to be missing due to low abundance or absence of the protein. In these cases, we chose to maintain the missing value as missing, assuming there is a biological reason for the absence. For this situation, we identified 212 proteins unique to nonsynaptic mitochondria and 325 proteins unique to synaptic mitochondria (Table S1E, Supporting Information). To determine if these proteins unique to one mitochondrial pool are associated with functions important for synaptic mitochondria we used the Database for Annotation, Visualization, and Integrated Discovery (DAVID) functional annotation tool for enrichment analysis and classified according to the Gene Ontology (GO) term biological process and found that the top five enriched biological processes were vesicle-mediated transport, synaptic transmission, protein localization, cell−cell signaling, and transmission of nerve impulse. In contrast, the top five enriched biological processes using DAVID based on nonsynaptic unique proteins were RNA processing, hexose metabolic process, cofactor metabolic process, glucose metabolic process, and energy derivation by oxidation of organic compounds.

dx.doi.org/10.1021/pr500295n | J. Proteome Res. 2014, 13, 2620−2636

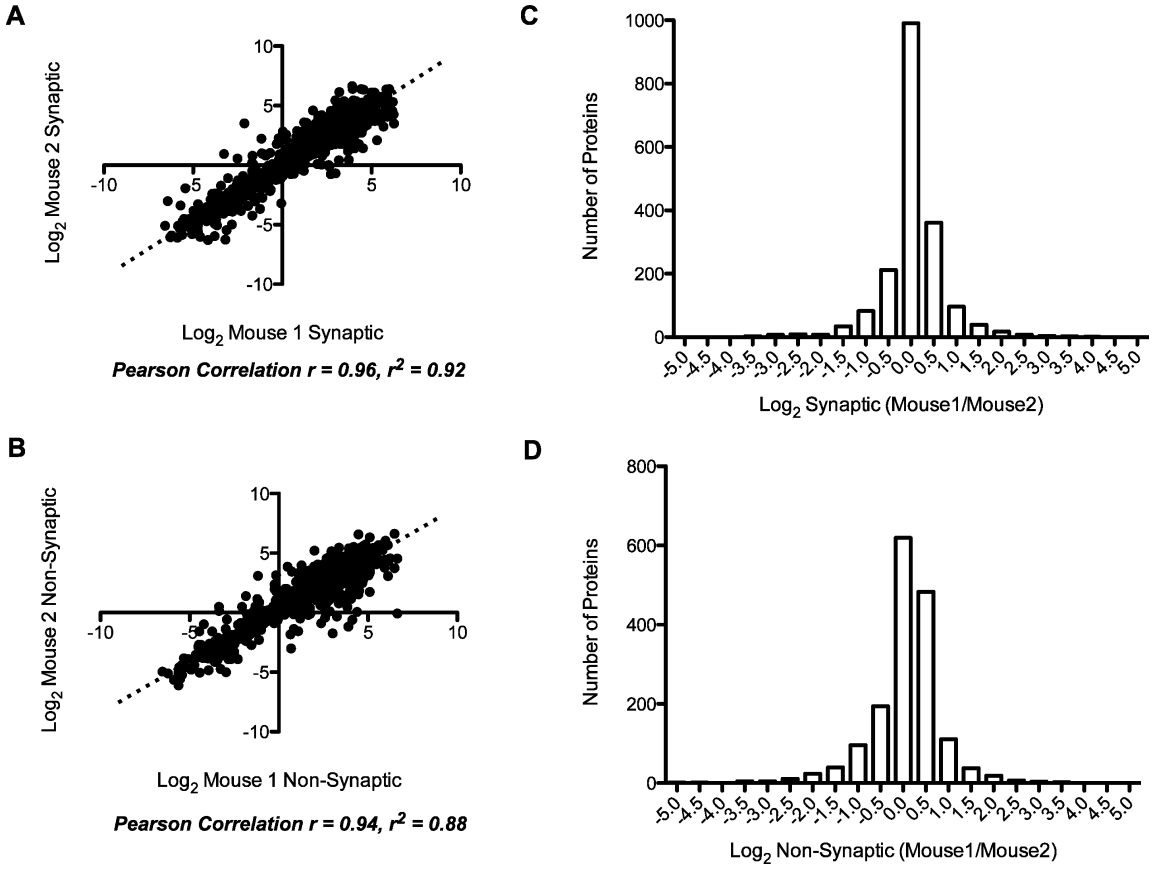

Figure 5. Experimental reproducibility and normalization. Scatter plot comparison of the normalized protein expression values determined in one biological replicate to another biological replicate analysis of proteins expressed in (A) synaptic and (B) nonsynaptic mitochondria. Histogram of protein ratios in one biological replicate versus another biological replicate for (C) synaptic and (D) nonsynaptic mitochondria.

Global Functional Assessment of Synaptic and Nonsynaptic Mitochondrial Proteins

In order to investigate the functional consequences of these proteomic changes in synaptic compared to nonsynaptic mitochondria, differentially expressed proteins were determined using the Bayesian regularization method for high-throughput differential analysis[26] of the 1278 identified mitochondrial proteins common between synaptic and nonsynaptic mitochondria (Figure 4D). The Posterior Probabilities of Differential Expression (PPDEs) were derived and Benjamini and Hochberg corrections were used. The resulting list of the 522 differentially expressed proteins between synaptic and nonsynaptic mitochondria quantified by super-SILAC are provided in Table S1F (Supporting Information). The 522 differentially expressed proteins were analyzed using the DAVID functional annotation tool for enrichment analysis and classified according to the GO terms cellular component, biological process, and molecular function. The GO analysis indicated that the list of differentially expressed proteins was enriched for mitochondrial proteins (Table 1). GO analysis of the differentially expressed mitochondrial proteins showed enrichment of biological processes related to generation of energy, metabolic processes, and protein translation (Table 1). In addition, the enrichment of molecular functions related to cofactor and nucleotide binding, inorganic cation transport, oxidoreductase activity, and ribosome components were observed (Table 1). Although just outside the top 10 biological processes, mitochondrion organization, which is of particular importance to mitochondrial function was also enriched. To further investigate these functional groups we used our proteomics data to investigate alterations in biological pathways relevant to energy production, mitochondrion organization, and transport of inorganic cations including oxidative phosphorylation (OXPHOS), mitochondrial fission/fusion, and calcium transport.

Decreased Expression of Electron-Transport Chain Subunits in Synaptic Compared to Nonsynaptic Mitochondria and Functional analysis

Since the analysis of the differentially regulated mitochondrial proteins using GO revealed enrichment of proteins involved in generation of energy pathways (Table 1), we further investigated the differential expression between synaptic and nonsynaptic mitochondria of the subunits of the protein complexes involved in the electron-transport chain (ETC) and OXPHOS. Interestingly, all of the subunits of the ETC that we identified, except for cytochrome c oxidase subunit IV isoform 2 (COX4I2), exhibit reduced expression in synaptic compared to nonsynaptic mitochondria (Figure 6A). Western blot analysis was used to orthogonally validate the decrease in expression of a subset of the ETC complex subunits (Figure 6B). The Western blot validation included at least one subunit from each ETC complex and revealed that ATP synthase subunit alpha (ATP5A1), cytochrome *b*-c1 complex subunit 2 (UQCRC2), cytochrome c oxidase subunit 1 (MTCO1), succinate dehydrogenase iron–sulfur subunit (SDHB), NADH dehydrogenase (ubiquinone) 1 β subcomplex subunit 8 (NDUFB8), and ATP synthase subunit d (ATP5H) were lower in synaptic versus nonsynaptic mitochondria consistent with our proteomics findings.

dx.doi.org/10.1021/pr500295n | J. Proteome Res. 2014, 13, 2620−2636

Table 1. Gene Ontology (GO) Annotation for Cellular Component, Biological Process, and Molecular Function Obtained from the Database for Annotation, Visualization, and Integrated Discovery (DAVID) for the 522 Accurately Quantified Differentially Expressed Proteins (P Value ≤0.05, PPDE ≥ 0.95, BH ≤ 0.05)

		% enrichment	P value
	GO: Cellular Component		
1	mitochondrion	81.8	$<8.5 \times 10^{-226}$
2	mitochondrial part	47.8	8.5×10^{-226}
3	mitochondrial envelope	31.1	2.6×10^{-127}
4	mitochondrial membrane	30.3	7.6×10^{-127}
5	mitochondrial inner membrane	27.8	5.4×10^{-126}
6	organelle inner membrane	28.2	1.1×10^{-124}
7	mitochondrial matrix	20.2	9.8×10^{-107}
8	mitochondrial lumen	20.2	9.8×10^{-107}
9	organelle envelope	31.9	4.9×10^{-106}
10	envelope	31.9	9.5×10^{-106}
	GO: Biological Process		
1	generation of precursor metabolites and energy	17.7	5.5×10^{-76}
2	oxidation reduction	22.8	2.0×10^{-62}
3	electron transport chain	10.4	2.2×10^{-52}
4	cellular respiration	5.8	1.3×10^{-29}
5	oxidative phosphorylation	5.0	2.4×10^{-24}
6	energy derivation by oxidation of organic compounds	6.0	3.0×10^{-23}
7	translation	9.6	1.3×10^{-22}
8	cofactor metabolic process	6.9	1.2×10^{-19}
9	coenzyme metabolic process	5.8	4.0×10^{-17}
10	acetyl-CoA metabolic process	3.1	9.3×10^{-16}
	GO: Molecular Function		
1	cofactor binding	9.4	7.1×10^{-28}
2	monovalent inorganic cation transmembrane transport	6.1	9.3×10^{-26}
3	hydrogen ion transmembrane transport	6.0	2.3×10^{-25}
4	oxidoreductase activity, acting on NADH or NADPH	5.0	3.3×10^{-25}
5	coenzyme binding	7.5	4.3×10^{-24}
6	oxidoreductase activity, acting on NADH or NADPH, quinone, or similar compound as acceptor	3.6	7.4×10^{-22}
7	NADH dehydrogenase (quinone) activity	3.5	2.0×10^{-21}
8	NADH dehydrogenase activity	3.5	2.0×10^{-21}
9	NADH dehydrogenase (ubiquinone) activity	3.5	2.0×10^{-21}
10	inorganic cation transmembrane transport	6.3	2.7×10^{-21}

In order to investigate the functional outcome of the observed proteomic changes, we used the Seahorse XF24 analyzer for sequential measurement of oxygen consumption rate using the isolated synaptic and nonsynaptic mitochondria.[30] In this assay with pyruvate and malate acting as substrates oxygen consumption by complex I is determined followed by inhibition with rotenone. Then complex II activity, driven by succinate, is measured followed by inhibition of complex III with antimycin A. Finally, ascorbate and TMPD are used to drive complex IV respiration. As shown in Figure 6C, the synaptic mitochondria exhibit significantly lower complex I, II, and IV driven respiration rates compared to nonsynaptic mitochondria consistent with the proteomics results. In response to stress (treatment with rotenone or antimycin A), both the synaptic and nonsynaptic mitochondrial oxygen consumption rates were similarly decreased (Figure S4, Supporting Information).

Differential Expression of Mitochondrial Fission/Fusion Proteins

As mentioned above, differentially expressed proteins were enriched for the process of mitochondrial organization. Therefore, we evaluated the expression of the proteins identified in our proteomic analysis that are involved in mitochondrial fission/fusion. As seen in Figure 7A, proteins involved in mitochondrial fission/fusion show differential expression in synaptic compared to nonsynaptic mitochondria. Specifically, dynamin-1-like protein (DNM1L), which is the regulator of mitochondrial fission, is increased ($\log_2 = 0.54$, $p = 0.022$, PPDE = 0.95, BH = 0.049) in synaptic compared to nonsynaptic mitochondria. Although predominantly cytoplasmic, DNM1L translocates to the mitochondria to mediate fission.[43] These results suggest a pro-fission state exists at the synapse. Consistent with this finding, proteins involved in both inner (dynamin-like 120 kDa protein; OPA1) and outer (mitofusin-1 and mitofusin-2; MFN1 and MFN2, respectively) mitochondrial membrane fusion are all reduced (OPA1: $\log_2 = -0.74$, $p = 0.000$, PPDE = 0.99, BH = 0.015) in synaptic compared to nonsynaptic mitochondria. The decreased protein level of MFN1 in synaptic mitochondria was validated orthogonally using Western blot analysis (Figure 7B).

Proteomic Implications for Altered Calcium Transport in Synaptic Mitochondria

The enrichment of proteins involved in the transport of inorganic cations was revealed based on GO analysis of the differentially expressed proteins in our proteomic analysis (Table 1). The homeostasis of calcium ions is specifically important at neuronal synapses so we examined the differential expression of proteins involved in calcium transport in synaptic compared to nonsynaptic mitochondria. We observed alterations in the expression of proteins important for calcium transport in our proteomics data (Figure 7C). Specifically, reduced expression of calcium uniporter protein (MCU: $\log_2 = -0.80$, $p = 0.001$, PPDE = 0.99, BH = 0.015) and calcium uptake protein 1 (MICU1: $\log_2 = -0.89$, $p = 0.001$, PPDE = 0.99, BH = 0.015) was found in synaptic mitochondria which is of particular interest since these proteins regulate mitochondrial calcium handling (Figure 7C).[44,45] Orthogonal validation using Western blotting showed that MCU protein levels were indeed lower in the synaptic compared to nonsynaptic mitochondria (Figure 7D).

Alterations in Transcriptional Regulation of Mitochondrial DNA-Encoded Proteins

The observation that all of the identified mitochondrial DNA (mtDNA) encoded ETC subunits showed decreased expression (Figure 6, Table 2) led us to examine the mtDNA transcriptional machinery. Mitochondrial RNA polymerase (POLRMT) and mitochondrial transcription factor A (TFAM) as well as either mitochondrial dimethyladenosine transferase 1 (TFB1M) or mitochondrial dimethyladenosine transferase 2 (TFB2M) are required for initiation of mtDNA transcription.[46] Additionally, the mitochondrial transcription termination factor (mTERF) facilitates termination of mtDNA transcription.[46] Our proteomics revealed that several proteins involved in mtDNA replication and expression were decreased

dx.doi.org/10.1021/pr500295n | J. Proteome Res. 2014, 13, 2620−2636

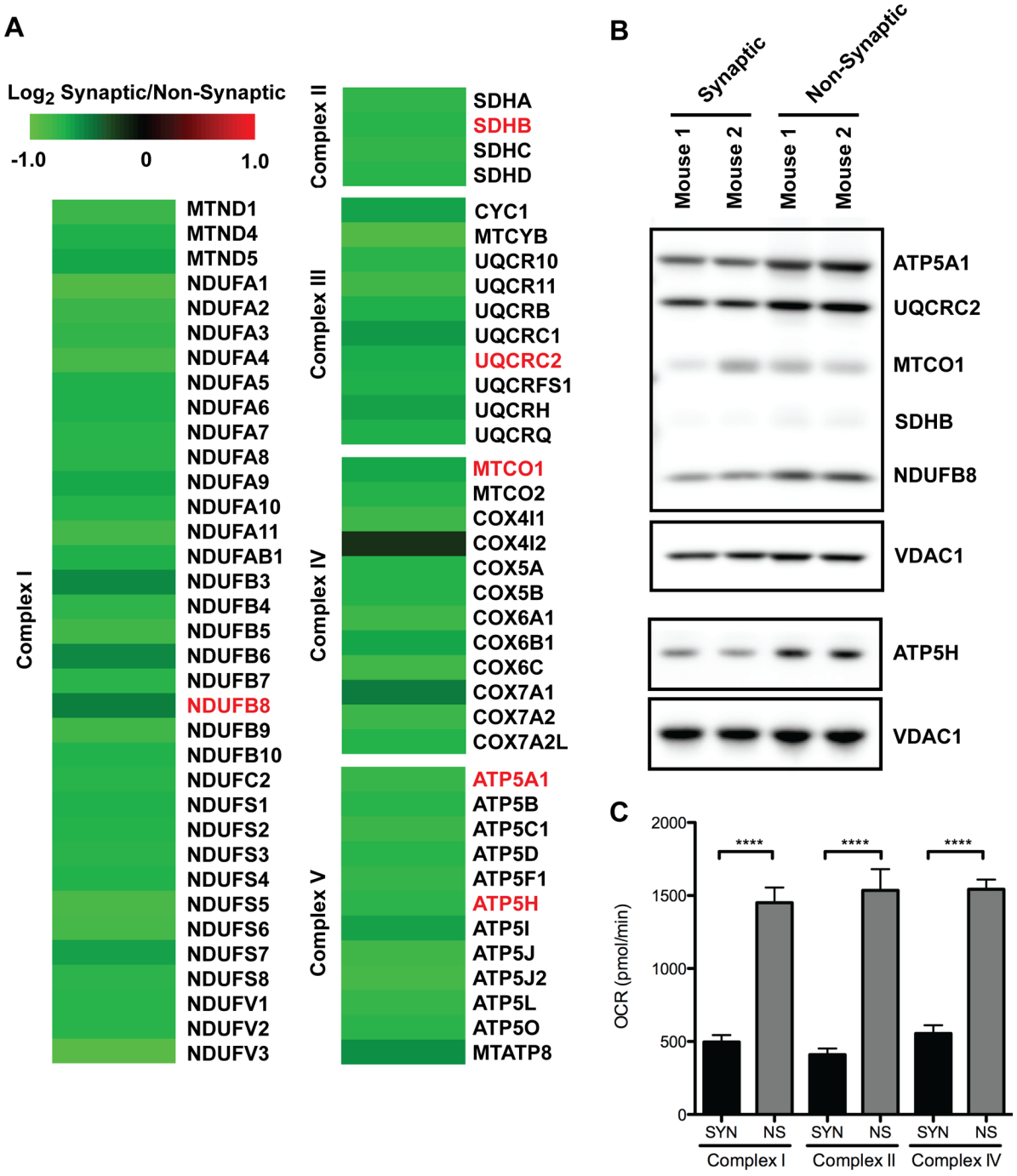

Figure 6. Down-regulation of electron transport chain complex subunits. (A) Heat map displaying the change in protein expression of mitochondrial electron transport chain complex subunits in synaptic from nonsynaptic mitochondria based on proteins quantified in the MS experiment. Proteins highlighted in red were verified orthogonally. The values are displayed on a $\log_2$ scale. (B) Western blot orthogonal validation of protein expression for several electron-transport chain subunits. VDAC1 is used as a loading control. (C) Seahorse XF24 electron flow assay showing complex I, II, and IV driven oxygen consumption rate (OCR) of synaptic and nonsynaptic mitochondria. Results are the mean ± SEM values (n = 6); synaptic (SYN) mitochondria are significantly (**** = $p < 0.0001$) different as compared with nonsynaptic (NS) mitochondria.

(POLRMT: $\log_2 = -1.02$, $p = 0.020$, PPDE = 0.95, BH = 0.046; SSBP1: $\log_2 = -0.71$, $p = 0.021$, PPDE = 0.95, BH = 0.048; TFAM: $\log_2 = -0.73$, $p = 0.004$, PPDE = 0.98, BH = 0.019) in synaptic compared to nonsynaptic mitochondria (Figure 8A). The decreased protein expression of TFAM was validated orthogonally via Western blotting (Figure 8B). Using IPA to investigate the TFAM transcriptional regulation network overlaid with our expression data, we observe that the downstream consequences of reduced TFAM levels are in line with our proteomics data, TFAM inhibited proteins are decreased and TFAM activated proteins are increased in synaptic mitochondria (Figure 8C). Since TFAM is responsible for transcriptional control of mtDNA, the finding of decreased TFAM expression is consistent with the observed reduced expression of mtDNA encoded proteins in synaptic mitochondria.

dx.doi.org/10.1021/pr500295n | J. Proteome Res. 2014, 13, 2620−2636

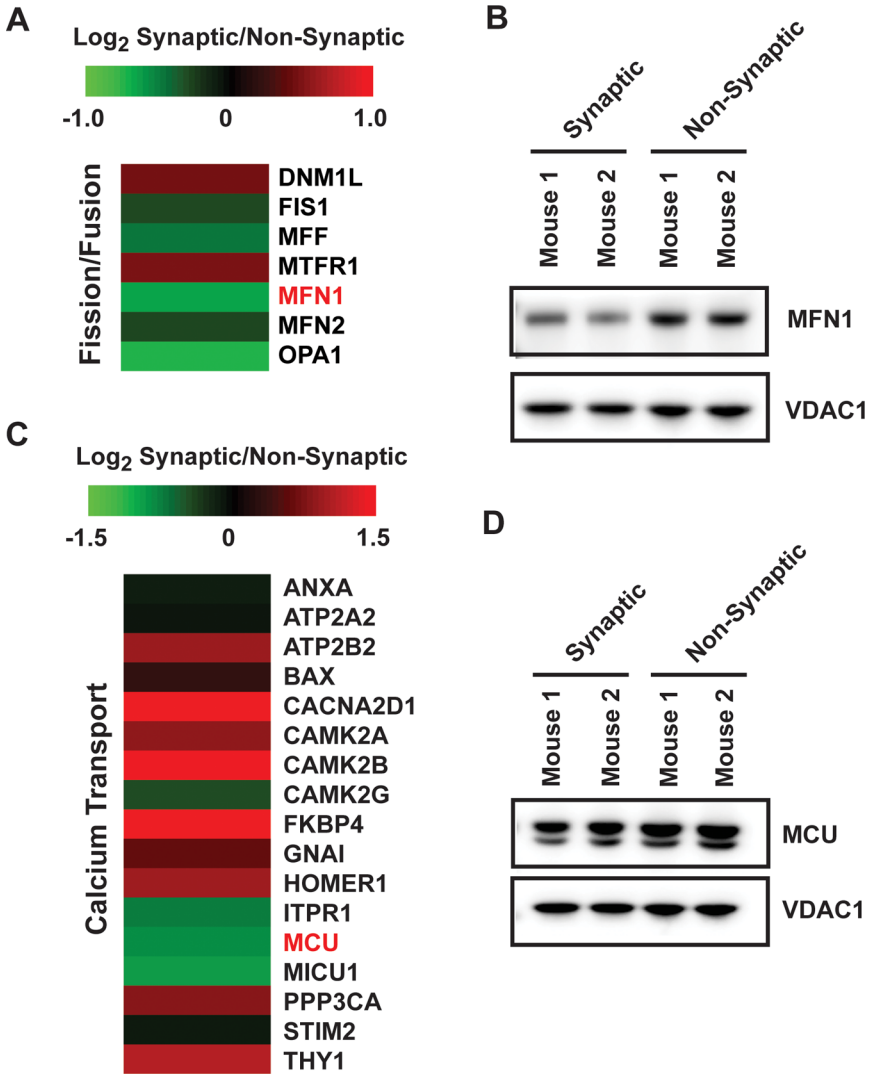

Figure 7. Differential expression of proteins involved in mitochondrial relevant pathways including fission/fusion and calcium transport. Heat map displaying the change in protein expression of (A) mitochondrial fission/fusion and (C) calcium transport proteins in synaptic from those in nonsynaptic mitochondria based on proteins quantitated in the MS experiment. Proteins highlighted in red were verified orthogonally. The values are displayed on a log2 scale. Western blot orthogonal validation of (B) MFN1 and (D) MCU expression.

Table 2. Mitochondrial DNA Encoded Proteins Quantified Using Super-SILAC Mix

		$\log_2$ (synaptic/nonsynaptic)			
protein names	gene names	replicate avg	joint analysis	*P* value	PPDE
MTATP8	ATP synthase protein 8	−0.61	−0.56	5.6×10^{-3}	0.98
MTCO1	cytochrome c oxidase subunit 1		−0.65		
MTCO2	cytochrome c oxidase subunit 2	−0.65	−0.71	1.2×10^{-3}	0.99
MTCYB	cytochrome *b*		−0.89		
MTND1	NADH-ubiquinone oxidoreductase chain 1	−0.75	−0.78	5.5×10^{-3}	0.98
MTND4	NADH-ubiquinone oxidoreductase chain 4	−0.68	−0.69	1.3×10^{-2}	0.97
MTND5	NADH-ubiquinone oxidoreductase chain 5	−0.60	−0.65	2.3×10^{-2}	0.95

Synaptic Mitochondria Exhibit an Increased Presence of Mitochondrial DNA Deletions

Multiple studies have shown age-dependent increases in mtDNA deletions in several different tissues and in many different species. Most mtDNA deletions are commonly found within regions flanked by short direct repeats as seen in the *Mus musculus* mitochondrion complete genome map (Figure 9A).[32,47] Since synaptic mitochondria are believed to be longer lived and to encounter more cellular stress, we chose to examine the extent of mtDNA deletions in synaptic compared to nonsynaptic mitochondria. PCR amplification of known age-associated mtDNA deletions was performed as described previously.[32] We observed an increased presence of mtDNA deletions found within the three-direct repeat region in synaptic compared to nonsynaptic mitochondria (Figure 9B). These deletions resulted in products of 989, 846, 753, 658, and 476 bp in length, which result from the mtDNA breakpoints 9554/13278, 9088/12956, 9262/13224, 8992/13049, and 8883/

dx.doi.org/10.1021/pr500295n | J. Proteome Res. 2014, 13, 2620−2636

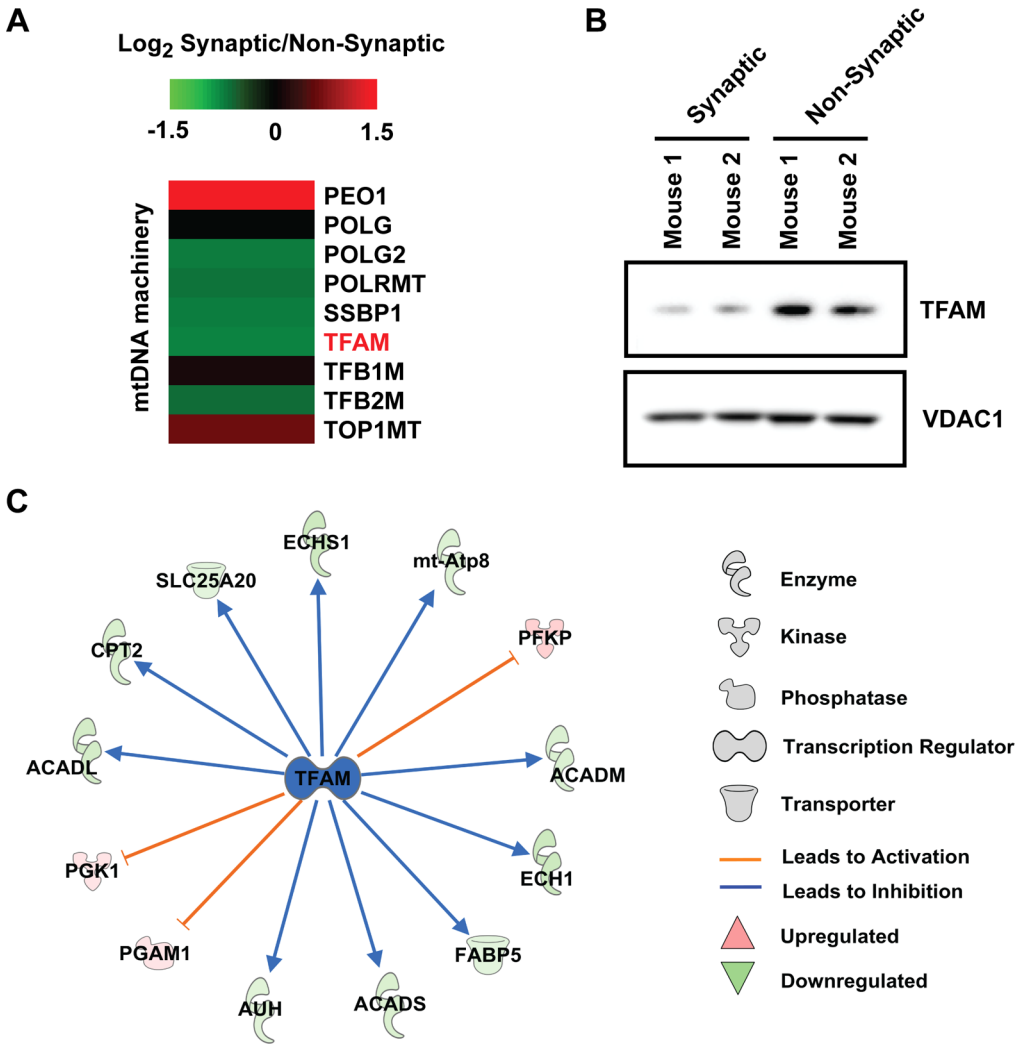

Figure 8. Mitochondrial DNA transcriptional regulation. (A) Heat map displaying the change in protein expression of mtDNA transcriptional machinery in synaptic from nonsynaptic mitochondria based on proteins quantified in the MS experiment. Proteins highlighted in red were verified orthogonally. The values are displayed on a $\log_2$ scale. (B) Western blot orthogonal validation of TFAM protein expression. (C) TFAM transcriptional regulator network from IPA.

13120, respectively (Figure 9B). This region of mtDNA contains coding sequence for five tRNAs (glycine (G), arginine (R), histidine (H), serine (S), and leucine (L)) and five ETC subunits (cytochrome c oxidase subunit 3 (COX3), NADH-ubiquinone oxidoreductase chain 3 (ND3), NADH-ubiquinone oxidoreductase chain 4L (ND4L), NADH-ubiquinone oxidoreductase chain 4 (ND4), and NADH-ubiquinone oxidoreductase chain 5 (ND5)). Therefore, increasing deletions within this region may contribute to the overall decreased expression of proteins encoded by mtDNA that we observed in synaptic as compared to nonsynaptic mitochondria (Table 2).

DISCUSSION

Mitochondrial functional and proteomic heterogeneity, which seems to be driven by the cellular environment, exists both between and within cells and tissues.[34,48,49] In addition to displaying increased susceptibility to damage compared to nonsynaptic mitochondria, studies have demonstrated that synaptic mitochondria are more vulnerable to cellular insults such as Ca^{2+} overload[12] and oxidative stress.[50] Although several studies have characterized the mouse brain synaptosomal proteome[51−53] and performed proteomic analysis of mouse brain synaptic proteins,[54,55] the mitochondrial proteome differences between synaptic and nonsynaptic mitochondria remain uncharacterized. In this study, we generated a super-SILAC mix that served as an appropriate internal standard for mouse brain mitochondria and performed a state of the art quantitative proteomic characterization of the mouse synaptic and nonsynaptic mitochondrial proteome at 10 months of age. This approach identified the differentially expressed proteins between synaptic and nonsynaptic mitochondria pointing to alterations in pathways important for function and integrity including OXPHOS, mitochondrial fission/fusion, calcium transport, and mitochondrial mtDNA replication and maintenance.

Our label-free proteomic analysis of mitochondria isolated from each of the four cell lines derived from mouse neural and glial origin, Neuro-2a, CATH.a, NB41A3, and C8-D1A, revealed that the use of a mixture of mitochondria isolated from these four cell lines increased proteome coverage and enabled representation of the mitochondrial proteome, due to mitochondrial protein enrichment (Figure 1 and 2). The creation of a super-SILAC mix from the four selected cell lines allowed for reproducible and accurate quantification of the

dx.doi.org/10.1021/pr500295n | J. Proteome Res. 2014, 13, 2620−2636

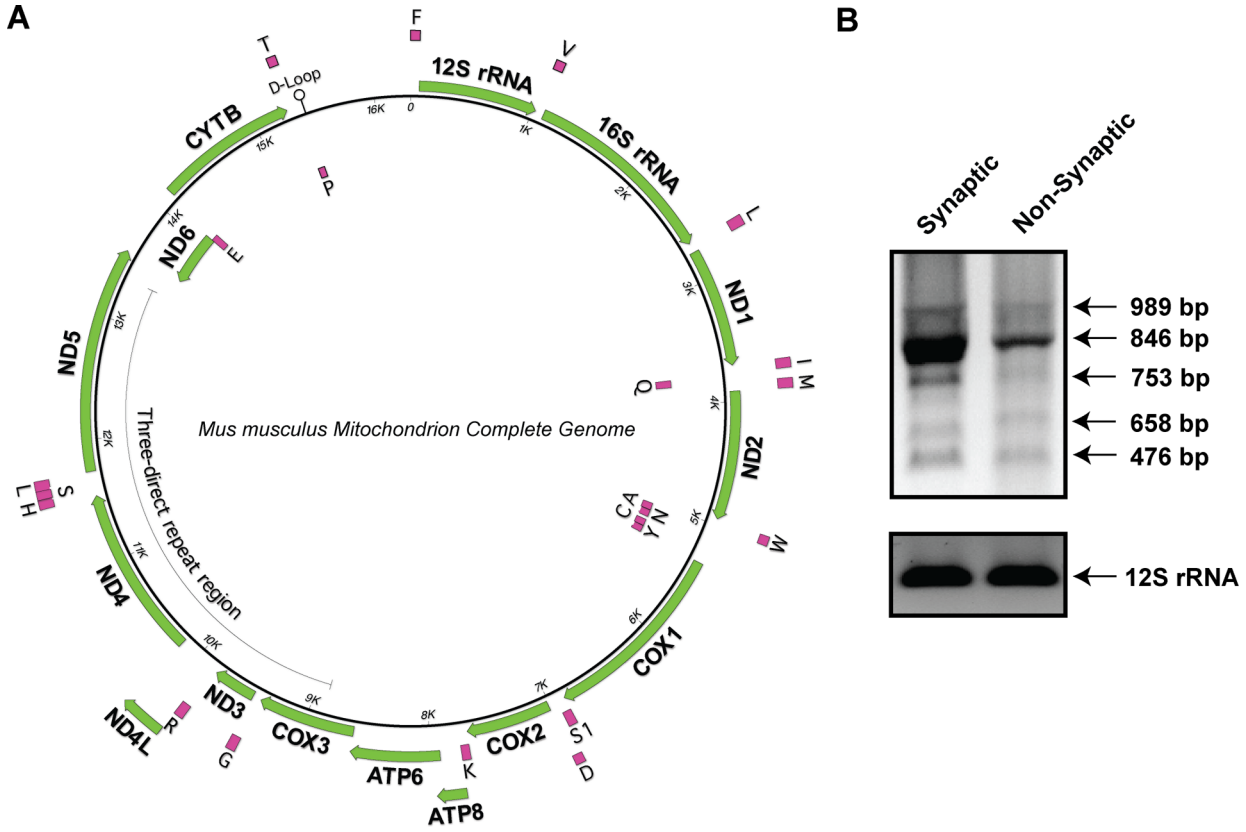

Figure 9. Mitochondrial DNA deletions. (A) Map of mouse mitochondrial DNA showing tRNA (pink), rRNA, and protein coding (green) regions. Areas prone to age-associated mutations are within the three-direct repeat region. (B) PCR analysis of DNA isolated from synaptic and nonsynaptic mitochondria revealing age-associated mitochondrial DNA deletions. PCR of 12S rRNA is used as a control.

proteomic differences between synaptic and nonsynaptic mitochondria isolated from 10-month-old mouse brains (Figures 3−5). In order to further predict how these proteomic changes may be associated with mitochondrial function and integrity, we used DAVID GO to determine the biological processes and molecular functions that are enriched using our list of 522 differentially regulated mitochondrial proteins. This analysis revealed proteins enriched in several pathways were differentially regulated between synaptic and nonsynaptic mitochondria (Table 1), specifically we chose to further investigate those essential for synaptic mitochondrial function including OXPHOS, mitochondrial fission/fusion, and calcium transport.

In particular, the synapse relies on high ATP production for vesicle mobilization and maintenance of membrane potential.[56] Therefore, we evaluated the proteomic changes associated with mitochondrial energy generation, the OXPHOS machinery. All of the subunits of the ETC that we identified, except for COX4I2, exhibited reduced expression in synaptic compared to nonsynaptic mitochondria which correlated with decreased complex I, II, and IV driven respiration (Figure 6). Given the demand for ATP at the synapse, this decrease in ETC complex subunits may be compensated for by trafficking of mitochondria resulting in a high density of mitochondria at the synapse.[4,57] Furthermore, decreases in mitochondrial ETC complex activities have been implicated in neurodegenerative diseases and aging, and our data provide evidence that the reduced activity may be a result of further proteomic alterations, as the reduced levels of the ETC complex subunits may make synaptic mitochondria more sensitive to such changes. In fact, synaptic mitochondria have been shown to exhibit more drastic reductions in rates of respiration and ATP production upon complex I inhibition compared to nonsynaptic mitochondria which was attributed to lower complex I activity in synaptic mitochondria.[58] Our data suggest that proteomic differences between synaptic and nonsynaptic mitochondria might explain these earlier findings, in that reduced expression of complex I subunits may contribute to the energy threshold whereby inhibition of mitochondrial OXPHOS would compromise energy homeostasis in the synapse and not near the neuronal soma.

Mitochondrial fission/fusion cycles are essential for the maintenance of mitochondrial integrity.[59] The observed alterations in the key proteins involved in regulating mitochondrial fission (increased DNM1L) and fusion (decreased OPA1, MFN1, and MFN2) suggest decreased fusion and the presence of increased fragmentation in the synaptic mitochondrial pool, which has been shown to result in decreased ATP production (Figure 7).[60] However, DNM1L not only controls fission but also mitochondrial localization to synapses regulating neuronal signaling.[61] Therefore, these proteomic alterations suggest that synaptic mitochondria may exhibit changes in morphology that could impact their function and integrity. However, further work is necessary to validate the functional consequences of DNM1L expression changes on mitochondrial morphology and localization. In fact, altered mitochondrial dynamics are implicated to contribute to the pathology of many neurodegenerative disorders including Parkinson's, Alzheimer's, and Huntington's diseases.[62,63]

dx.doi.org/10.1021/pr500295n | J. Proteome Res. 2014, 13, 2620−2636

In addition to producing ATP, mitochondria are necessary for maintaining proper calcium homeostasis at the neuronal synapse.[61] Interestingly, synaptic mitochondria display increased susceptibility to calcium-induced dysfunction and calcium overload compared to nonsynaptic mitochondria.[12,16] Mitochondrial calcium uptake is mediated by a calcium-selective ion channel,[45] and the pore-forming subunit MCU was recently shown to interact with MICU1, which was shown to be essential to prevent mitochondrial calcium overload.[44] Our proteomics revealed that the expression of both MCU and MICU1 is decreased in synaptic compared to nonsynaptic mitochondria (Figure 7). Interestingly, synaptic activity has been shown to transcriptionally repress MCU which prevents excitotoxic death.[64] Therefore, although reduced MCU expression (as observed by our proteomics) would be expected to be beneficial for survival, this may also leave the synaptic mitochondria more susceptible to calcium overload.

Based on our proteomic expression data, all of the ETC complex subunits encoded by mtDNA show reduced expression in synaptic compared to nonsynaptic mitochondria (Figure 6; Table 2). Consistent with this finding, the mtDNA transcriptional machinery including TFAM, the master regulator of transcription for the mitochondrial genome, was reduced in synaptic compared to nonsynaptic mitochondria (Figure 8). The IPA upstream regulators tool revealed that decreased levels of TFAM were also consistent with the observed protein expression levels of other downstream targets (Figure 8). In addition to mtDNA transcription, TFAM is also recruited to mitochondria for mtDNA maintenance and biogenesis.[65] Therefore, decreased levels of TFAM may contribute to synaptic mitochondrial increased sensitivity to damage and reduced integrity.

Since synaptic mitochondria have been shown to be especially vulnerable to cumulative age-associated damage,[13] we investigated the presence of mtDNA damage. Our finding of increased synaptic mitochondrial mtDNA deletions compared to nonsynaptic mitochondria supports other findings that synaptic mitochondria are more vulnerable to age-related damage (oxidative or otherwise) (Figure 9). Interestingly, recent studies have revealed that most mtDNA mutations in aged cells appear to be caused by early replication errors which propagate with time;[66] thus, this finding also supports the idea that synaptic mitochondria are longer lived than nonsynaptic.

CONCLUSIONS

Here we have characterized the differences between synaptic and nonsynaptic mitochondria using a quantitative proteomics approach. Our work indicates that global proteomic differences exist between synaptic and nonsynaptic mitochondria. Synaptic mitochondria exhibit distinct protein expression indicative of decreased energy generation, as well as altered mitochondrial morphology and calcium transport compared to their nonsynaptic counterparts. Our findings suggest changes in the mitochondrial proteome could explain the observed vulnerability of synaptic mitochondria to inhibitors of ETC complexes, calcium, as well as age-associated damage. We identified an increase in the presence of mtDNA damage coinciding with decreased TFAM levels in synaptic compared to nonsynaptic mitochondria. We hypothesize that some of the same proteomic alterations that allow synaptic mitochondria to provide for the unique demands of synapses may also lead to synaptic mitochondrial vulnerability. This study provides the basis for further experiments on the role of synaptic mitochondrial proteins in neurodegenerative disorders as well as normal aging.

ASSOCIATED CONTENT

Supporting Information

Figure S1: confirmation of equal loading for Western blot. Figure S2: similarity of the mitochondria isolated from the four cell lines based on label-free proteomics. Figure S3: purification of synaptic and nonsynaptic mitochondria. Figure S4: decreased rate of oxygen consumption in synaptic compared to nonsynaptic mitochondria. Table S1A: complete spectral count data for all proteins identified using mitochondria isolated from each of the four cell lines. Table S1B: MitoMiner annotated proteins identified using mitochondria isolated from each of the four cell lines. Table S1C: complete super-SILAC data for all proteins identified using nonsynaptic and synaptic mitochondria isolated from mouse 1 and 2. Table S1D: complete super-SILAC data for all proteins identified as in common between nonsynaptic and synaptic mitochondria isolated from mouse 1 and 2. Table S1E: proteins identified as unique due to missing values in another sample. Table S1F: differentially expressed proteins between synaptic and nonsynaptic mitochondria quantified by super-SILAC. This material is available free of charge via the Internet at http://pubs.acs.org.

AUTHOR INFORMATION

Corresponding Author

*E-mail: hfox@unmc.edu. Phone: (402) 559-4821. Fax: (402) 559-7495.

Author Contributions

The manuscript was written through contributions of all authors.

Funding

This research was supported by the National Institute of Health Grant Nos. P30 MH062261 and R01 MH073490.

Notes

The authors declare no competing financial interest.

ACKNOWLEDGMENTS

We are grateful to the following University of Nebraska Medical Center Core Facilities for assistance with data generation: the Mass Spectrometry and Proteomics Core Facility especially Dr. Pawel Ciborowski and Melinda Wojtkiewicz; and the Electron Microscopy Core Facility particularly Tom Barger (Department of Genetics, Cell Biology, and Anatomy). We thank Dr. Robert Lewis for the use of the Seahorse Analyzer.

ABBREVIATIONS

SILAC, stable isotope labeling with amino acids in cell culture; IM, isolation medium; ATM, atmospheric; TTOF, triple time-of-flight; MS, mass spectrometry; LC, liquid chromatography; FDR, false discovery rate; L/H, light/heavy; GO, gene ontology; ETC, electron transport chain; OXPHOS, oxidative phosphorylation; FASP, filter-aided sample preparation; DAVID, Database for Annotation, Visualization, and Integrated Discovery; IPA, ingenuity pathway analysis; DNM1L, dynamin-1-like; OPA1, dynamin-like 120 kDa protein; MCU, calcium uniporter protein; MICU1, calcium uptake protein 1; MFN1,

mitofusin-1; MFN2, mitofusin-2; TFAM, mitochondrial transcription factor A; mtDNA, mitochondrial DNA

REFERENCES

(1) Waagepetersen, H. S.; Hansen, G. H.; Fenger, K.; Lindsay, J. G.; Gibson, G.; Schousboe, A. Cellular mitochondrial heterogeneity in cultured astrocytes as demonstrated by immunogold labeling of alpha-ketoglutarate dehydrogenase. *Glia* **2006**, *53* (2), 225−31.

(2) Kuznetsov, A. V.; Margreiter, R. Heterogeneity of mitochondria and mitochondrial function within cells as another level of mitochondrial complexity. *Int. J. Mol. Sci.* **2009**, *10* (4), 1911−29.

(3) Li, Z.; Okamoto, K.; Hayashi, Y.; Sheng, M. The importance of dendritic mitochondria in the morphogenesis and plasticity of spines and synapses. *Cell* **2004**, *119* (6), 873−87.

(4) Chang, D. T.; Honick, A. S.; Reynolds, I. J. Mitochondrial trafficking to synapses in cultured primary cortical neurons. *J. Neurosci.* **2006**, *26* (26), 7035−45.

(5) Billups, B.; Forsythe, I. D. Presynaptic mitochondrial calcium sequestration influences transmission at mammalian central synapses. *J. Neurosci.* **2002**, *22* (14), 5840−7.

(6) Verstreken, P.; Ly, C. V.; Venken, K. J.; Koh, T. W.; Zhou, Y.; Bellen, H. J. Synaptic mitochondria are critical for mobilization of reserve pool vesicles at Drosophila neuromuscular junctions. *Neuron* **2005**, *47* (3), 365−78.

(7) Evans, R. J.; Derkach, V.; Surprenant, A. ATP mediates fast synaptic transmission in mammalian neurons. *Nature* **1992**, *357* (6378), 503−5.

(8) Chen, H.; Chan, D. C. Mitochondrial dynamics—fusion, fission, movement, and mitophagy—in neurodegenerative diseases. *Hum. Mol. Genet.* **2009**, *18* (R2), R169−76.

(9) DiMauro, S.; Schon, E. A. Mitochondrial disorders in the nervous system. *Annu. Rev. Neurosci.* **2008**, *31*, 91−123.

(10) Hollenbeck, P. J. The pattern and mechanism of mitochondrial transport in axons. *Front Biosci* **1996**, *1*, d91−102.

(11) Tong, J. J. Mitochondrial delivery is essential for synaptic potentiation. *Biol. Bull.* **2007**, *212* (2), 169−75.

(12) Brown, M. R.; Sullivan, P. G.; Geddes, J. W. Synaptic mitochondria are more susceptible to Ca2+overload than nonsynaptic mitochondria. *J. Biol. Chem.* **2006**, *281* (17), 11658−68.

(13) Martinez, M.; Hernandez, A. I.; Martinez, N.; Ferrandiz, M. L. Age-related increase in oxidized proteins in mouse synaptic mitochondria. *Brain Res.* **1996**, *731* (1−2), 246−8.

(14) Naga, K. K.; Sullivan, P. G.; Geddes, J. W. High cyclophilin D content of synaptic mitochondria results in increased vulnerability to permeability transition. *J. Neurosci.* **2007**, *27* (28), 7469−75.

(15) Du, H.; Guo, L.; Yan, S.; Sosunov, A. A.; McKhann, G. M.; Yan, S. S. Early deficits in synaptic mitochondria in an Alzheimer's disease mouse model. *Proc. Natl. Acad. Sci. U.S.A.* **2010**, *107* (43), 18670−5.

(16) Yarana, C.; Sanit, J.; Chattipakorn, N.; Chattipakorn, S. Synaptic and nonsynaptic mitochondria demonstrate a different degree of calcium-induced mitochondrial dysfunction. *Life Sci.* **2012**, *90* (19−20), 808−14.

(17) Battino, M.; Gorini, A.; Villa, R. F.; Genova, M. L.; Bovina, C.; Sassi, S.; Littarru, G. P.; Lenaz, G. Coenzyme Q content in synaptic and non-synaptic mitochondria from different brain regions in the ageing rat. *Mech. Ageing Dev.* **1995**, *78* (3), 173−87.

(18) Deeb, S. J.; D'Souza, R. C.; Cox, J.; Schmidt-Supprian, M.; Mann, M. Super-SILAC allows classification of diffuse large B-cell lymphoma subtypes by their protein expression profiles. *Mol. Cell Proteomics* **2012**, *11* (5), 77−89.

(19) Geiger, T.; Cox, J.; Ostasiewicz, P.; Wisniewski, J. R.; Mann, M. Super-SILAC mix for quantitative proteomics of human tumor tissue. *Nat. Methods* **2010**, *7* (5), 383−5.

(20) Geiger, T.; Wehner, A.; Schaab, C.; Cox, J.; Mann, M. Comparative proteomic analysis of eleven common cell lines reveals ubiquitous but varying expression of most proteins. *Mol. Cell Proteomics* **2012**, *11* (3), M111 014050.

(21) Kristian, T., Isolation of mitochondria from the CNS. *Curr. Protoc. Neurosci.* **2010**, Chapter 7, Unit 7 22.

(22) Chelli, B.; Falleni, A.; Salvetti, F.; Gremigni, V.; Lucacchini, A.; Martini, C. Peripheral-type benzodiazepine receptor ligands: mitochondrial permeability transition induction in rat cardiac tissue. *Biochem. Pharmacol.* **2001**, *61* (6), 695−705.

(23) Wisniewski, J. R.; Zougman, A.; Nagaraj, N.; Mann, M. Universal sample preparation method for proteome analysis. *Nat. Methods* **2009**, *6* (5), 359−62.

(24) Scopes, R. K. Measurement of protein by spectrophotometry at 205 nm. *Anal. Biochem.* **1974**, *59* (1), 277−82.

(25) Shilov, I. V.; Seymour, S. L.; Patel, A. A.; Loboda, A.; Tang, W. H.; Keating, S. P.; Hunter, C. L.; Nuwaysir, L. M.; Schaeffer, D. A. The Paragon Algorithm, a next generation search engine that uses sequence temperature values and feature probabilities to identify peptides from tandem mass spectra. *Mol. Cell Proteomics* **2007**, *6* (9), 1638−55.

(26) Kayala, M. A.; Baldi, P. Cyber-T web server: differential analysis of high-throughput data. *Nucleic Acids Res.* **2012**, *40* (Web Server issue), W553−9.

(27) Huang, D. W.; Sherman, B. T.; Lempicki, R. A. Systematic and integrative analysis of large gene lists using DAVID bioinformatics resources. *Nat. Protoc.* **2009**, *4*, 44−57.

(28) Ferguson, R. E.; Carroll, H. P.; Harris, A.; Maher, E. R.; Selby, P. J.; Banks, R. E. Housekeeping proteins: a preliminary study illustrating some limitations as useful references in protein expression studies. *Proteomics* **2005**, *5* (2), 566−71.

(29) Yuqi, L.; Lei, G.; Yang, L.; Zongbin, L.; Hua, X.; Lin, W.; Rui, C.; Mohan, L.; Yi, W.; Minxin, G.; Shiwen, W. Voltage-dependent anion channel (VDAC) is involved in apoptosis of cell lines carrying the mitochondrial DNA mutation. *BMC Med. Genet* **2009**, *10*, 114.

(30) Rogers, G. W.; Brand, M. D.; Petrosyan, S.; Ashok, D.; Elorza, A. A.; Ferrick, D. A.; Murphy, A. N. High throughput microplate respiratory measurements using minimal quantities of isolated mitochondria. *PloS One* **2011**, *6* (7), e21746.

(31) Gerencser, A. A.; Neilson, A.; Choi, S. W.; Edman, U.; Yadava, N.; Oh, R. J.; Ferrick, D. A.; Nicholls, D. G.; Brand, M. D. Quantitative microplate-based respirometry with correction for oxygen diffusion. *Anal. Chem.* **2009**, *81* (16), 6868−78.

(32) Wang, E.; Wong, A.; Cortopassi, G. The rate of mitochondrial mutagenesis is faster in mice than humans. *Mutat. Res.* **1997**, *377* (2), 157−66.

(33) Grimsrud, P. A.; Carson, J. J.; Hebert, A. S.; Hubler, S. L.; Niemi, N. M.; Bailey, D. J.; Jochem, A.; Stapleton, D. S.; Keller, M. P.; Westphall, M. S.; Yandell, B. S.; Attie, A. D.; Coon, J. J.; Pagliarini, D. J. A quantitative map of the liver mitochondrial phosphoproteome reveals posttranslational control of ketogenesis. *Cell Metab.* **2012**, *16* (5), 672−83.

(34) Forner, F.; Kumar, C.; Luber, C. A.; Fromme, T.; Klingenspor, M.; Mann, M. Proteome differences between brown and white fat mitochondria reveal specialized metabolic functions. *Cell Metab.* **2009**, *10* (4), 324−35.

(35) Jiang, Y.; Wang, X. Comparative mitochondrial proteomics: perspective in human diseases. *J. Hematol. Oncol.* **2012**, *5*, 11.

(36) Rhee, H. W.; Zou, P.; Udeshi, N. D.; Martell, J. D.; Mootha, V. K.; Carr, S. A.; Ting, A. Y. Proteomic mapping of mitochondria in living cells via spatially restricted enzymatic tagging. *Science* **2013**, *339* (6125), 1328−31.

(37) Flurkey, K, C, J., Harrison, D. E., The mouse in aging research. In *The Mouse in Biomedical Research*, 2nd ed.; Fox, J. G., Ed.; American College of Laboratory Animal Medicine (Elsevier): Burlington, MA, 2007; Vol *III*, Normative Biology, Husbandry, and Models, pp 637−672.

(38) Lifshitz, J.; Friberg, H.; Neumar, R. W.; Raghupathi, R.; Welsh, F. A.; Janmey, P.; Saatman, K. E.; Wieloch, T.; Grady, M. S.; McIntosh, T. K. Structural and functional damage sustained by mitochondria after traumatic brain injury in the rat: evidence for differentially sensitive populations in the cortex and hippocampus. *J. Cereb. Blood Flow Metab.* **2003**, *23* (2), 219−31.

(39) Pagliarini, D. J.; Calvo, S. E.; Chang, B.; Sheth, S. A.; Vafai, S. B.; Ong, S. E.; Walford, G. A.; Sugiana, C.; Boneh, A.; Chen, W. K.; Hill, D. E.; Vidal, M.; Evans, J. G.; Thorburn, D. R.; Carr, S. A.; Mootha, V.

K. A mitochondrial protein compendium elucidates complex I disease biology. *Cell* **2008**, *134* (1), 112−23.
(40) Valledor, L.; Jorrin, J. Back to the basics: Maximizing the information obtained by quantitative two dimensional gel electrophoresis analyses by an appropriate experimental design and statistical analyses. *J. Proteomics* **2011**, *74* (1), 1−18.
(41) Pedreschi, R.; Hertog, M. L.; Carpentier, S. C.; Lammertyn, J.; Robben, J.; Noben, J. P.; Panis, B.; Swennen, R.; Nicolai, B. M. Treatment of missing values for multivariate statistical analysis of gel-based proteomics data. *Proteomics* **2008**, *8* (7), 1371−83.
(42) Little, R. J. A.; Rubin, D. B. *Statistical Analysis with Missing Data*; John Wiley: New York, 2002.
(43) Smirnova, E.; Griparic, L.; Shurland, D. L.; van der Bliek, A. M. Dynamin-related protein Drp1 is required for mitochondrial division in mammalian cells. *Mol. Biol. Cell* **2001**, *12* (8), 2245−56.
(44) Mallilankaraman, K.; Doonan, P.; Cardenas, C.; Chandramoorthy, H. C.; Muller, M.; Miller, R.; Hoffman, N. E.; Gandhirajan, R. K.; Molgo, J.; Birnbaum, M. J.; Rothberg, B. S.; Mak, D. O.; Foskett, J. K.; Madesh, M. MICU1 is an essential gatekeeper for MCU-mediated mitochondrial Ca(2+) uptake that regulates cell survival. *Cell* **2012**, *151* (3), 630−44.
(45) Kirichok, Y.; Krapivinsky, G.; Clapham, D. E. The mitochondrial calcium uniporter is a highly selective ion channel. *Nature* **2004**, *427* (6972), 360−4.
(46) Leigh-Brown, S.; Enriquez, J. A.; Odom, D. T. Nuclear transcription factors in mammalian mitochondria. *Genome Biol.* **2010**, *11* (7), 215.
(47) Samuels, D. C.; Schon, E. A.; Chinnery, P. F. Two direct repeats cause most human mtDNA deletions. *Trends Genet.* **2004**, *20* (9), 393−8.
(48) Lotz, C.; Lin, A. J.; Black, C. M.; Zhang, J.; Lau, E.; Deng, N.; Wang, Y.; Zong, N. C.; Choi, J. H.; Xu, T.; Liem, D. A.; Korge, P.; Weiss, J. N.; Hermjakob, H.; Yates, J. R., III; Apweiler, R.; Ping, P. Characterization, Design, and Function of the Mitochondrial Proteome: From Organs to Organisms. *J. Proteome Res.* **2014**, *13* (2), 433−46.
(49) Villeneuve, L.; Tiede, L. M.; Morsey, B.; Fox, H. S. Quantitative proteomics reveals oxygen-dependent changes in neuronal mitochondria affecting function and sensitivity to rotenone. *J. Proteome Res.* **2013**, *12* (10), 4599−606.
(50) Banaclocha, M. M.; Hernandez, A. I.; Martinez, N.; Ferrandiz, M. L. N-Acetylcysteine protects against age-related increase in oxidized proteins in mouse synaptic mitochondria. *Brain Res.* **1997**, *762* (1−2), 256−8.
(51) Filiou, M. D.; Bisle, B.; Reckow, S.; Teplytska, L.; Maccarrone, G.; Turck, C. W. Profiling of mouse synaptosome proteome and phosphoproteome by IEF. *Electrophoresis* **2010**, *31* (8), 1294−301.
(52) Flynn, J. M.; Czerwieniec, G. A.; Choi, S. W.; Day, N. U.; Gibson, B. W.; Hubbard, A.; Melov, S. Proteogenomics of synaptosomal mitochondrial oxidative stress. *Free Radic. Biol. Med.* **2012**, *53* (5), 1048−60.
(53) Schrimpf, S. P.; Meskenaite, V.; Brunner, E.; Rutishauser, D.; Walther, P.; Eng, J.; Aebersold, R.; Sonderegger, P. Proteomic analysis of synaptosomes using isotope-coded affinity tags and mass spectrometry. *Proteomics* **2005**, *5* (10), 2531−41.
(54) Tweedie-Cullen, R. Y.; Reck, J. M.; Mansuy, I. M. Comprehensive mapping of post-translational modifications on synaptic, nuclear, and histone proteins in the adult mouse brain. *J. Proteome Res.* **2009**, *8* (11), 4966−82.
(55) Sidhu, V. K.; Huang, B. X.; Kim, H. Y. Effects of docosahexaenoic acid on mouse brain synaptic plasma membrane proteome analyzed by mass spectrometry and (16)O/(18)O labeling. *J. Proteome Res.* **2011**, *10* (12), 5472−80.
(56) Murthy, V. N.; De Camilli, P. Cell biology of the presynaptic terminal. *Annu. Rev. Neurosci.* **2003**, *26*, 701−28.
(57) Shepherd, G. M.; Harris, K. M. Three-dimensional structure and composition of CA3→CA1 axons in rat hippocampal slices: implications for presynaptic connectivity and compartmentalization. *J. Neurosci.* **1998**, *18* (20), 8300−10.
(58) Davey, G. P.; Peuchen, S.; Clark, J. B. Energy thresholds in brain mitochondria. Potential involvement in neurodegeneration. *J. Biol. Chem.* **1998**, *273* (21), 12753−7.
(59) Youle, R. J.; van der Bliek, A. M. Mitochondrial fission, fusion, and stress. *Science* **2012**, *337* (6098), 1062−5.
(60) Lutz, A. K.; Exner, N.; Fett, M. E.; Schlehe, J. S.; Kloos, K.; Lammermann, K.; Brunner, B.; Kurz-Drexler, A.; Vogel, F.; Reichert, A. S.; Bouman, L.; Vogt-Weisenhorn, D.; Wurst, W.; Tatzelt, J.; Haass, C.; Winklhofer, K. F. Loss of parkin or PINK1 function increases Drp1-dependent mitochondrial fragmentation. *J. Biol. Chem.* **2009**, *284* (34), 22938−51.
(61) Sheng, Z. H.; Cai, Q. Mitochondrial transport in neurons: impact on synaptic homeostasis and neurodegeneration. *Nat. Rev. Neurosci* **2012**, *13* (2), 77−93.
(62) Itoh, K.; Nakamura, K.; Iijima, M.; Sesaki, H. Mitochondrial dynamics in neurodegeneration. *Trends Cell Biol.* **2013**, *23* (2), 64−71.
(63) Correia, S. C.; Santos, R. X.; Perry, G.; Zhu, X.; Moreira, P. I.; Smith, M. A. Mitochondrial importance in Alzheimer's, Huntington's and Parkinson's diseases. *Adv. Exp. Med. Biol.* **2012**, *724*, 205−21.
(64) Qiu, J.; Tan, Y. W.; Hagenston, A. M.; Martel, M. A.; Kneisel, N.; Skehel, P. A.; Wyllie, D. J.; Bading, H.; Hardingham, G. E. Mitochondrial calcium uniporter Mcu controls excitotoxicity and is transcriptionally repressed by neuroprotective nuclear calcium signals. *Nat. Commun.* **2013**, *4*, 2034.
(65) Seibenhener, M. L.; Du, Y.; Diaz-Meco, M. T.; Moscat, J.; Wooten, M. C.; Wooten, M. W. A role for sequestosome 1/p62 in mitochondrial dynamics, import and genome integrity. *Biochim. Biophys. Acta* **2013**, *1833* (3), 452−9.
(66) Lopez-Otin, C.; Blasco, M. A.; Partridge, L.; Serrano, M.; Kroemer, G. The hallmarks of aging. *Cell* **2013**, *153* (6), 1194−217.